Topological quenching of spin tunneling in magnetic molecules with a fourfold easy axis

Chang-Soo Park* and Anupam Garg†
Department of Physics and Astronomy, Northwestern University, Evanston, Illinois 60208
(Received 13 July 2001; published 15 January 2002)

Spin tunneling is investigated in magnetic molecules that have an easy axis with fourfold symmetry, such as Mn_{12}-acetate, with emphasis on understanding the topological quenching of tunneling and the diabolical point locations in the magnetic field space. This is done using a model spin Hamiltonian that has a fourth-order term describing the tetragonal anisotropy. The problem is studied qualitatively using instantons and quantitatively using two methods: a discrete phase integral or Wentzel-Kramers-Brillouin method and perturbation theory in the fourth-order anisotropy and transverse magnetic field. The former method is used to find the splitting between various levels when the applied magnetic field is along the hard axis and is found to give good quantitative answers. The latter method is employed for fields which may have an easy component in addition to a hard one and is found to be effective in locating all the diabolical points. These points are found as the roots of a small number of polynomials in the hard component of the magnetic field and the basal plane anisotropy. These roots are used to obtain approximate formulas that apply to any system with total spin $S \leqslant 10$. The analytic results are found to compare reasonably well with exact numerical diagonalization for the case of Mn_{12}-acetate. In addition, perturbation theory shows that the diabolical points may be indexed by the magnetic quantum numbers of the levels involved, even at large transverse fields. Certain points of degeneracy are found to be mergers (or near mergers) of two or three diabolical points because of the symmetry of the problem.

DOI: 10.1103/PhysRevB.65.064411 PACS number(s): 75.10.Dg, 03.65.Db, 03.65.Sq, 75.45.+j

I. INTRODUCTION

Quantum tunneling of a spin or spinlike degree of freedom has been discussed for over a decade now,[1] but unambiguous evidence for its existence has only come recently[2] from studies on the magnetic molecule $[Fe_8O_2(OH)_{12}(tacn)_6]^{8+}$ (Fe_8 for short). This molecule has a total spin $S=10$, is biaxially symmetric, and can be modeled by the spin Hamiltonian

$$\mathcal{H}=k_1S_x^2+k_2S_y^2-g\mu_B\mathbf{S}\cdot\mathbf{H}, \tag{1.1}$$

with $k_1>k_2>0$. In the first approximation, it has two degenerate ground states, approximately given by $S_z=\pm 10$, which are separated by an energy barrier in the *xy* plane. The question of interest is to understand how these states are admixed by quantum tunneling.

Direct numerical diagonalization of Eq. (1.1) using the experimentally determined values $k_1\simeq 0.33$ K and $k_2 \simeq 0.22$ K (Ref. 3–5) reveals that the tunnel splitting Δ is $\sim 10^{-9}$ K, which is too small to be observed directly. Wernsdorfer and Sessoli[2] overcome this difficulty by applying a small amplitude ac magnetic field along the *z* direction, which causes the $S_z=\pm 10$ levels to cross one another. Transitions between these levels are now possible via the Landau-Zener-Stückelberg (LZS) process,[6] and the underlying tunneling matrix element Δ can be deduced from a measurement of the incoherent LZS relaxation rate for the total magnetization. The key experimental fact that supports this interpretation of the relaxation (which could after all be due to a classical activation process a priori) is a systematic and remarkable oscillatory dependence of the inferred splitting Δ on the strength of the magnetic field $\mathbf{H}$ when this field is applied along the hard direction $\hat{\mathbf{x}}$. One way of understanding this behavior is in terms of interference of different Feynman tunneling paths for spin,[7] and this is how it was theoretically discovered.[8] While massive particle tunneling in two or more spatial dimensions can also show such interference,[9] the effect arises more directly in the spin problem since the kinetic term in the action has the mathematical structure of a Berry phase. Briefly, when $\mathbf{H}\|\hat{\mathbf{x}}$, there are two symmetry-related instanton paths that wind around $\hat{\mathbf{x}}$ in opposite directions and together form a closed loop on the (complexified) unit sphere. The actions for the instantons are complex and differ by a real-valued Berry phase given by *S* times the area of the loop, giving rise to interference. Since the Berry phase may be continuously varied by varying *H*, the splitting oscillates as a function of *H*, being completely quenched at values of *H* where the Berry phase is an odd integer times π.

In addition to being quenched for fields along the hard axis, the splitting is also quenched at other isolated points in the H_x-H_z plane. These quenchings do not have as visual an explanation as that given above, but they are ultimately due to the Berry-phase-like term in the spin path integral. (One could equally well say that they are due to the spin commutators being what they are.) We note that *all* these quenching points are *diabolical* points in the terminology of Berry and Wilkinson[10] or *conical intersections* in older terminology.[11] These differences between massive particle and spin tunneling add to the interest in the problem. Reciprocally, the experiments on Fe_8 have spurred more careful investigations of spin-coherent-state path integrals which are more delicate than their massive particle counterparts.[12]

A second magnetic molecule Mn_{12}-acetate (or Mn_{12}-ac for short) has also been the subject of several experimental studies.[13–18] The reason for our interest in Mn_{12}-ac is that it

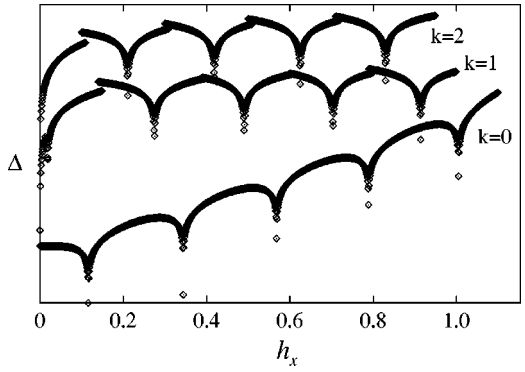

FIG. 1. Semilogarithmic plot of numerically calculated splittings between the levels $m=-10$ and $m=10-k$ for $k=0,1$, and 2, as a function of $h_x=g\mu_B H_x/AS$. The scale on the y axis has been omitted as it is arbitrary, and the $k=1$ curves have been vertically offset for clarity. For $k=0$, $h_z=g\mu_B H_z/AS=0$ all throughout, while for $k=1$, h_z is 0.135 836 224, 0.135 832 551, 0.135 027, 0.133 225, 0.130 354, and 0.126 331 for the successive quenches, and for $k=2$, successive quenches are at h_z equal to 0.264 938, 0.263 958, 0.261 042, 0.256 130, and 0.249 084. As discussed in Sec. IV C, there are two extremely close by diabolical points near $h_x=0$ for $k=1$ and two merged diabolical points for $k=2$.

has a different symmetry from Fe_8. In the presence of an external magnetic field **H**, the spin Hamiltonian of Mn_{12}-ac can be written as

$$\mathcal{H}=-AS_z^2-BS_z^4+C(S_+^4+S_-^4)-g\mu_B\mathbf{H}\cdot\mathbf{S}, \qquad (1.2)$$

where $A\gg B\gg C>0$. The easy axis z now has fourfold symmetry, the hard axes are $\pm x$ and $\pm y$, and the medium axes are the lines $y=\pm x$ in the xy plane. Here, the symmetry of a pair of instanton paths is preserved when a magnetic field is applied along one of the four hard axes. Thus, the quenched spin tunneling phenomenon is also expected to occur in systems with this symmetry. To our knowledge, the effect has not been seen in Mn_{12}-ac to date, but the issue of its observability in any particular system is one that depends on many other factors, in particular the scale of the splitting and the strength and nature of the environmental decoherence. It is not the purpose of this paper to discuss these questions. We shall only study the quenching effect in the idealized system described by the Hamiltonian (1.2). Given the large variety of magnetic molecules being studied and synthesized,[19] one may hope that a system will be found in which the effect can indeed be observed.

Because of the differences in symmetry, the systematics of the quenching effect in tetragonal systems are different from those in Fe_8. One of the main differences is shown in Fig. 1. We show the numerically computed splittings between Zeeman levels with quantum numbers $m=-10$ and $m'=10-k$ for $k=0$, 1, and 2, using values of A, B, and C that are appropriate to Mn_{12}-ac (for which see below). This figure should be compared with Fig. 2B of Ref. 2. As can be seen, here too the appropriate splitting is quenched at certain values of the magnetic field. However, the pattern of the quenching points—their locations and their number as a function of k—is not so simple as in Fe_8. Second, in the simplest model for Fe_8, the quenching points for given $k\neq 0$ all have the same easy-axis field H_z.[20] Here this is not so. Another way of saying this is that in the H_x-H_z plane, the quenching points for given k no longer lie on lines parallel to the x axis. This means that to search for these points experimentally, one must scan along lines or curves that have a slight negative slope with respect to the x axis. As we shall see, the tunneling matrix element in the vicinity of a quenching point depends very sharply on H_z, and this is why we have shown the quenchings in Fig. 1 as a sequence of H_x scans at different H_z values. This need not be too severe a problem for an experimental search, however, if the method of Wersndorfer and Sessoli[2] is employed. In this approach, the H_z field has a small ac component. As long as the ac amplitude is large enough to pass through a crossing somewhere in the cycle, its exact location does not matter. From this point of view, it continues to make sense to think of Δ for a given pair of levels as depending principally on H_x.

It is clearly of interest to try and understand the above properties of the Hamiltonian (1.2) and, more broadly, the full tunneling spectrum, analytically. Ideally, one would like expressions or methods for calculating Δ for any pair of levels for any external magnetic field **H** (assuming of course that **H** is such that the levels are quasidegenerate to begin with). A secondary goal might be to obtain the locations of the quenching points. We report progress toward both these goals using two separate methods. The first is the discrete phase integral (DPI) (or discrete WKB) method.[21–25] This method has been applied to spin tunneling problems in several recent papers by one of us,[26–28] and an approximate version of it has been developed and applied to the specific case of Fe_8 by Villain and Fort.[29] It is semiclassical just as the instanton approach is, but it is easier to use for the study of the splittings of higher pairs of levels and when the magnetic field is not along a hard axis. The calculation reduces to the evaluation of a handful of action integrals. Unlike the Fe_8 case, however, these integrals must now be evaluated numerically. This means that we do not have explicit analytic formulas for Δ and the value of the exercise is somewhat reduced for general **H**. Therefore, our DPI studies are limited to the case $\mathbf{H}\|\hat{\mathbf{x}}$. For general field orientations, we use perturbation theory in H_x and the ratio C/A, very much in the spirit of Ref. 30. To our pleasant surprise, this not only yields quite good approximations for the locations of the diabolical points, it also reveals a pattern in the points which would be hard to discern otherwise. This pattern provides a natural scheme for indexing these points.

Some readers may wonder why an analytic study of Eq. (1.2) is needed at all, since the corresponding 21×21 matrix may be diagonalized numerically.[31,32] First, there have also been many other semiclassical studies of the Fe_8 system in the last two years[33] using a variety of analytic methods—periodic instantons, Bohr-Sommerfeld quantization, mapping on to a particle,[34] etc., but none of these is easily applicable to the Mn_{12}-ac symmetry. Second, numerical methods are undoubtedly invaluable, but they cannot by themselves provide one with mental pictures or language with which to interpret physical phenomena, understand trends, or yield

any of the insights that one means when one talks of the ''physics'' of a problem. In the present problem it is very unlikely that numerics alone would have led to the indexing scheme we find. Third, any black-box numerical routine must itself have an analytic basis. Standard methods such as tridiagonalization followed by QR factorization[35] are inferior to the DPI for calculating tunnel splittings, especially if the spin is large. As J increases, the splitting decreases exponentially, so one needs exponentially more significant digits in a numerical approach. The DPI method tackles the problem of calculating this exponentially small quantity head on. Thus we believe that even if the answers for Eq. (1.2) are known numerically, it is of some value to see how well they can be captured by an analytic approach. Such a comparison especially serves as a test of the DPI method and increases one's confidence in applying it in situations where numerics are not feasible.

The plan of our paper is as follows. In the following section we give a qualitative discussion of spin tunneling based on instantons and selection rules. This gives an overall picture of the quenching systematics and sets the stage for the more detailed analyses to follow.

In Sec. III we present the DPI formalism for the present model. Unlike the previously studied model for Fe_8, the Schrödinger equation corresponding to the present spin Hamiltonian becomes a nine-term recursion relation because of the fourth-order term. Hence, although the formalism of Ref. 27 does not need to be extended (see especially the discussion of nonclassical turning points therein), the actual application is made more difficult due to the nine terms. We give a systematic analysis for this recursion relation. We then calculate the tunnel splittings as a function of the applied field for the first few energy levels and compare our results with those from numerical diagonalization.

The perturbative analysis is given in Sec. IV. We first develop the perturbation theory with $B=0$ (Sec. IV A). This yields the diabolical points as the roots of polynomials in H_x and C. For a given spin S, we have $2S$ polynomials. One of the unexpected bonuses is that a polynomial which applies to a given value of S also applies to any other value of S. We find all these polynomials for $S \leqslant 10$. In Sec. IV B, we incorporate the effects of the B term approximately and compare our analytic results with those from explicit numerical diagonalization of the Hamiltonian with the parameters for Mn_{12}-ac. Our results are accurate to about 10%, and we believe that they will also be useful for other systems with fourfold anisotropy. This is especially true for the low-lying energy levels. In fact, for the higher pairs of levels, the diabolical points can be significantly moved or even eliminated altogether by still higher ansitropy terms in the Hamiltonian. In Sec. IV C we discuss some qualitative aspects of the degeneracies on the H_z axis and show that some of them behave as the merger of two or three diabolical points. Our main results from perturbation theory are in the form of tables of the underlying polynomials and explicit diabolical fields for Mn_{12}-ac. Because of their length, we have placed these tables in the EPAPS depository.[36]

We conclude the paper with a summary of the results in Sec. V.

II. QUALITATIVE ARGUMENTS

We begin with a qualitative treatment of spin tunneling in Mn_{12}-ac using instanton methods, considering only $\mathbf{H}\|\hat{\mathbf{x}}$. This method is based on spin-coherent-state path integrals. In the spin-coherent-state representation the anisotropy energy corresponding to the Hamiltonian (1.2), with $\mathbf{H}\|\hat{\mathbf{x}}$, is given by

$$\begin{aligned}\mathcal{H}_c(\alpha,\beta) = \langle \hat{\mathbf{n}}|\mathcal{H}|\hat{\mathbf{n}}\rangle = &-AS^2\sin^2\alpha\sin^2\beta - BS^4\sin^4\alpha\sin^4\beta \\ &+ 2CS^4(\cos^4\alpha + \sin^4\alpha\cos^4\beta \\ &- 6\sin^2\alpha\cos^2\alpha\cos^2\beta) - g\mu_B H_x S\cos\alpha, \quad (2.1)\end{aligned}$$

where α and β are the polar and azimuthal angles with respect to $\hat{\mathbf{x}}$, i.e.,

$$(\hat{\mathbf{n}}_\mathbf{x},\hat{\mathbf{n}}_\mathbf{y},\hat{\mathbf{n}}_\mathbf{z}) = (\cos\alpha, \sin\alpha\cos\beta, \sin\alpha\sin\beta). \quad (2.2)$$

In Eq. (2.1), we have omiited terms of relative order $(1/S)$. The energy (2.1) exhibits two degenerate minima at $\hat{\mathbf{n}}_i = (\alpha,\beta) = (\alpha_0, \pi/2)$ and $\hat{\mathbf{n}}_f = (\alpha,\beta) = (\alpha_0, -\pi/2)$, where $\alpha_0 = \pi/2$ for $H_x = 0$, and decreases smoothly to 0 as H_x is increased. The level splitting due to tunneling between these minima can be obtained from the imaginary time propagator

$$K_{fi} = \langle \hat{\mathbf{n}}_f|\exp[-\mathcal{H}T]|\hat{\mathbf{n}}_i\rangle = \int \mathcal{D}[\hat{\mathbf{n}}]\exp\{-S_E[\hat{\mathbf{n}}(\tau)]\}, \quad (2.3)$$

where

$$S_E[\hat{\mathbf{n}}(\tau)] = -iS\mathcal{A}[\hat{\mathbf{n}}(\tau)] + \int_0^T \mathcal{H}_c(\alpha,\beta)d\tau, \quad (2.4)$$

with

$$\mathcal{A}[\hat{\mathbf{n}}(\tau)] = \int_0^T (1-\cos\alpha)\dot{\beta}(\tau)d\tau \quad (2.5)$$

the Euclidean action and complex in general. Here, the boundary conditions are $\hat{\mathbf{n}}(0) = \hat{\mathbf{n}}_i, \hat{\mathbf{n}}(T) = \hat{\mathbf{n}}_f$. Geometrically, for a closed path, the integral in Eq. (2.5) can be interpreted as a surface area on the complexified unit sphere enclosed by this path, as can be verified by the Stokes theorem. In the large-spin limit the path integral can be approximated by the sum of all contributions from paths that minimize the action: that is, the instanton paths. The instantons for the present model are not simple because of the fourth-order terms. However, we can construct a qualitative argument to find the quenching effect without performing explicit calculations. Since the Euclidean action S_E has both real and imaginary parts we can express the ground-state tunnel splitting as

$$\Delta = \sum_j D_j e^{-S_{Rj}} e^{iS_{Ij}}, \quad (2.6)$$

where j labels the various instantons, S_{Rj} and S_{Ij} are the real and imaginary parts of the instanton action, respectively, and D_j are prefactors. With these ingredients we now discuss how the quenching appears in the present model.

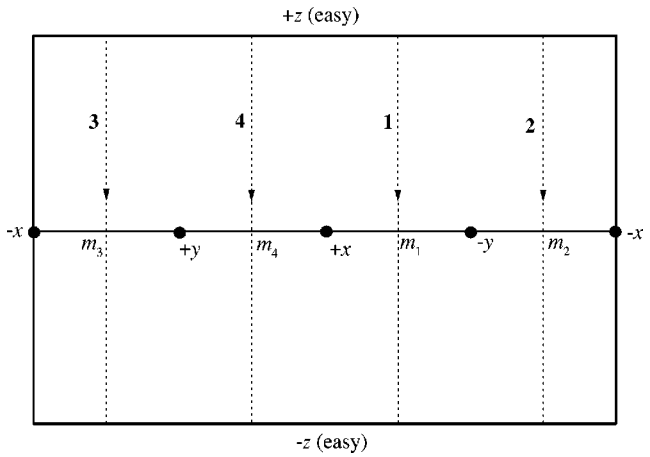

FIG. 2. Two-dimensional picture of instanton paths when $H_x=0$. The points $\pm x$, $\pm y$ are the hard axes, and m_i's represent the medium axes. Dotted lines denote the real projections of the instanton paths.

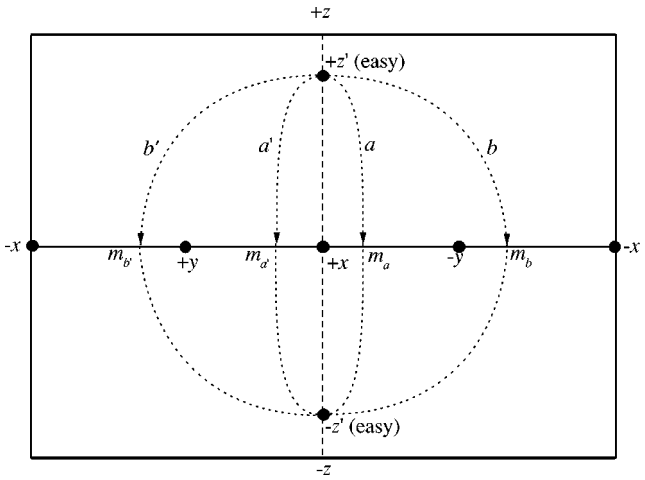

FIG. 3. Two-dimensional picture of instanton paths when $H_x\neq 0$. The points $\pm z'$ represent the new easy axes. The instanton paths are again denoted by dotted lines. Note that the areas enclosed by each pair of instanton paths are shrunk due to the field.

Let us first consider the case when $H_x=0$. Since the energy has fourfold symmetry, an argument of von Delft and Henley can be applied.[7] If $\hat{\mathbf{n}}(\tau)$ is an instanton path, so is $\mathcal{R}_{\hat{\mathbf{z}}}(\pi/2)\hat{\mathbf{n}}(\tau)$, where $\mathcal{R}_{\hat{\mathbf{z}}}(\pi/2)$ is a rotation through $\pi/2$ about $\hat{\mathbf{z}}$. Keeping in mind that $\hat{\mathbf{n}}(\tau)$ is complex, when we project onto the real unit sphere, there are four saddle-point paths passing through each of the four medium directions. Because of symmetry, each has the same real contribution to the action integral S_R. However, since their azimuths about the easy axis are different, the imaginary part of the action, i.e., the phase S_I, will not be the same. From the geometrical meaning of the integral in Eq. (2.5), the phase difference between two instanton paths equals S times the surface area on the unit sphere enclosed by these instanton paths.

To visualize the interference effect we map the two-sphere onto a plane, as in an ordinary atlas (see Fig. 2). The hard axes are mapped onto four equally separated points lying on the equator, and the points exactly halfway between these correspond to the medium axes. Thus, the real projections of the instanton paths can be drawn as curves which start from $+z$, pass through the medium points, and end at $-z$. The area enclosed by two adjacent instanton paths equals π, since the sphere is equally divided into four parts by the instantons. Thus, the phase difference between adjacent paths becomes $S\pi$. Choosing the phase of path 1 as the base, we can perform the summation in Eq. (2.6). Recalling that by symmetry the contribution from real parts of the instanton actions are the same, as are the prefactors D_j, we have

$$\Delta = De^{-S_R}e^{-iS_I}(1+e^{-i\pi S}+e^{-2i\pi S}+e^{-3i\pi S})$$
$$=4De^{-S_R}e^{i\gamma}\cos(\pi S)\cos\left(\frac{\pi S}{2}\right), \tag{2.7}$$

where γ is an irrelevant phase. This result gives us two quenching conditions. From the factor $\cos\pi S$, we obtain the quenching of spin tunneling for half-integer S, which is just the Kramers degeneracy effect. The second cosine implies that the ground-state spin tunneling is quenched for odd integer spins, i.e., $S=1,\ 3,\ 5$, etc., and so Δ is non-zero only for $S=2p$, where p is an integer.[37]

We now consider the case with $H_x\neq 0$. Since the field is assumed to be applied along the $+x$ axis, both easy and all four medium axes move close to the $+x$ axis. Thus, the two-dimensional picture becomes the one shown in Fig. 3. The fourfold symmetry is now broken, but there are two pairs of instanton paths surrounding the $+x$ axis: (a,a') and (b,b'). The real parts of the instanton actions in a pair are the same, but different between the pairs. The phase differences in each pair are the areas enclosed by each pair of instanton paths (the small and large oval regions in Fig. 3) and are dependent on the field H_x. If we choose the straight line joining $+z'$ to $-z'$ as a reference, $S_{Ia'}=-S_{Ia}, S_{Ib'}=-S_{Ib}$, so that the summation in Eq. (2.6) can be performed as

$$\Delta = D_a e^{-S_{Ra}}[e^{-iS_{Ia}}+e^{-iS_{Ia'}}]+D_b e^{-S_{Rb}}[e^{-iS_{Ib}}+e^{-iS_{Ib'}}]$$
$$=2D_a e^{-S_{Ra}}\cos\frac{SA_a(H_x)}{2}+2D_b e^{-S_{Rb}}\cos\frac{SA_b(H_x)}{2}, \tag{2.8}$$

where S_{Ra} and S_{Rb} are the real parts of the instanton actions in each pair, and $A_a(H_x)$ and $A_b(H_x)$ are the areas enclosed by the pairs (a,a') and (b,b'), respectively. For $H_x>0$ the saddle points through which the paths (a,a') pass are lower than those for (b,b'), which means that $S_{Ra}<S_{Rb}$. The main contribution to Δ in Eq. (2.8) then comes from the first term, and we can neglect the second term. The quenching of the ground-state tunnel splitting thus arises when $A_a(H_x)\simeq(2n+1)\pi/S$, where n is a non-negative integer. To see how many quenching points are allowed we note that $A_a(H_x)<A_a(0)$, where $A_a(0)=\pi$ (the area enclosed by the two paths 1 and 4 in Fig. 2). From this condition we find $n<(S-1)/2$. For $S=10$ there are thus five values of H_x at which the quenching appears.

It should be noted that the region of very small (but non-zero) H_x is special. Exactly at $H_x=0$, four instantons are

important, but for large H_x only two are important. There must therefore be a regime of small H_x where we make a smooth transition between these two behaviors. The width of this regime can be quite small since $S_{Rb} > S_{Ra}$ as soon as $H_x \neq 0$, and these actions appear in the exponents in Eq. (2.8), so that the difference $(S_{Rb} - S_{Ra})$ is amplified. It is to be expected that treating this crossover region correctly is a technical problem in asymptotics requiring some kind of uniform asymptotic approximation. We shall see that the difficulty persists in the DPI treatment. In particular, the basic formula (3.29) fails near $H_x = 0$. It contains only one cosine factor and is effectively ignoring the second term in Eq. (2.8).

It does not seem easy to generalize this qualitative argument for the number of diabolical points when $H_z \neq 0$ and the tunneling involves an excited state in at least one well. In particular, there is no simple argument that an area of π is lost for each excited state, as one might be tempted to think based on the simplicity of the diabolical point pattern in Fe_8.

It is possible to understand the spectrum when $\mathbf{H} = 0$ or when $\mathbf{H} \| \hat{\mathbf{z}}$ in terms of a selection rule induced by the fourth-order terms in Eq. (1.2). First, as also noted by Tupitsyn and Barbara,[32] when $\mathbf{H} = 0$, the splitting between levels $-10 + n$ and $10 - n$ alternates between zero and nonzero as the level pair number n goes up. The $S_{\pm}^4$ terms forbid transitions between levels m and m' unless $\Delta m = |m - m'|$, is a multiple of 4. For tunneling between levels m and $-m$, this requires $2m = 4p$, where p is an integer, so there is no such tunneling when m is an odd number.

To give a more detailed argument of this point, we note that when $\mathbf{H} \| \hat{\mathbf{z}}$, the $S_{\pm}^4$ terms divide the Hamiltonian into the following four subspaces for $S = 10$:

$$V_1 = \{-10, -6, -2, +2, +6, +10\},$$

$$V_2 = \{-9, -5, -1, +3, +7\},$$

$$V_3 = \{-8, -4, 0, +4, +8\},$$

$$V_4 = \{-7, -3, +1, +5, +9\}, \tag{2.9}$$

where the numbers in brackets give the m quantum numbers. The subspace V_1 contains 6 levels, which form 3 pairs split by tunneling due to the $CS_{\pm}^4$ terms. The space V_3 contains 5 levels, of which ± 8 and ± 4 are split by tunneling and $m = 0$ is isolated. There is no degeneracy amongst the states in any one subspace. At $\mathbf{H} = 0$, however, the space V_2 is isomorphic to V_4 by time reversal symmetry, and we therefore conclude that in the full spectrum of $\mathcal{H}$, there should be five pairs of *strictly* degenerate levels, corresponding approximately to $m = \pm(2n+1)$ with integer n. Further, we can also see that as H_z is turned on, states in different subspaces will cross. Thus, the level -10 in V_1 will cross successively with $+9, +8$, and $+7$ since these are in V_4, V_3, and V_2, but it will not cross with $+6$ since that level is also in V_1.

III. DPI CALCULATION OF TUNNEL SPLITTINGS

We consider the spin Hamiltonian (1.2) with the magnetic field applied along the x axis. For convenience we divide $\mathcal{H}$ by A to work with dimensionless quantities. With this choice we can write

$$\mathcal{H} = -S_z^2 - \lambda_1 S_z^4 + \lambda_2 [S_+^4 + S_-^4] - \overline{Sh}_x S_x, \tag{3.1}$$

where $\lambda_1 = B/A, \lambda_2 = C/A, \overline{h}_x = H_x/\overline{S} H_c (H_c \equiv A/g\mu_B)$, and

$$\overline{S} = S + \frac{1}{2}. \tag{3.2}$$

Here, μ_B is the Bohr magneton, $g = 2$, and S is the spin. Following Ref. 17, $A/k_B = 0.556$ K, $B/k_B = 1.1 \times 10^{-3}$ K, and $C/k_B = 3 \times 10^{-5}$ K, so that $\lambda_1 = 1.98 \times 10^{-3}$, $\lambda_2 = 5.4 \times 10^{-5}$, and $H_c = 0.414$ T. Let $|\hat{\mathbf{n}}\rangle = |\theta, \phi\rangle$ be the spin-coherent state along the direction $\hat{\mathbf{n}}$, with standard spherical polar coordinates θ and ϕ. We introduce the classical energy

$$\begin{aligned} \mathcal{H}_c(\theta, \phi) &= \langle \hat{\mathbf{n}} | \mathcal{H} | \hat{\mathbf{n}} \rangle \\ &= -S^2 \cos^2\theta - \lambda_1 S^4 \cos^4\theta \\ &\quad + 2\lambda_2 S^4 \sin^4\theta \cos 4\phi - S\overline{Sh}_x \sin\theta \cos\phi. \end{aligned} \tag{3.3}$$

When $\overline{h}_x = 0$, $\mathcal{H}_c$ has minima at $\theta = 0, \theta = \pi$. As $\overline{h}_x$ is increased, these minima move toward $\theta = \pi/2$, $\phi = 0$, lying in the xz plane. At a certain critical field $\overline{h}_{xco}$, these minima will merge with each other, giving rise to a double zero of $\partial \mathcal{H}_c(\theta, \phi = 0)/\partial\theta$ at $\theta = \pi/2$. By using this condition, we can show that

$$\overline{h}_{xco} = \frac{2S}{\overline{S}}(1 + 4\lambda_2 S^2). \tag{3.4}$$

With the experimental numbers given above, $\overline{h}_{xco} = 1.946$.[38]

A. Recursion relation

The DPI formalism can be started with the Schrödinger equation in the S_z representation. Introducing $\mathcal{H}|\psi\rangle = E|\psi\rangle$, $S_z|m\rangle = m|m\rangle$, $\langle m|\psi\rangle = C_m$, and $\langle m|\mathcal{H}|m'\rangle = t_{m,m'}$, the Schrödinger equation for the Hamiltonian (1.2) can be expressed as

$$\sum_{n=m-4}^{m+4} t_{m,n} C_n = E C_m. \tag{3.5}$$

This is a nine-term recursion relation with diagonal terms $t_{m,m}$ from S_z^2 and S_z^4 and off-diagonal terms $t_{m,m\pm1}, t_{m,m\pm,4}$ which are from the S_x and $S_{\pm}^4$ parts, respectively. Since there are no $S_{\pm}^2$ or $S_{\pm}^3$ terms in the Hamiltonian, we have $t_{m,m\pm2} = t_{m,m\pm3} = 0$.

Equation (3.5) may be interpreted as the Schrödinger equation of an electron in a one-dimensional tight binding model. That is, we can consider the diagonal and off-diagonal terms as the on-site energy and hopping terms, re-

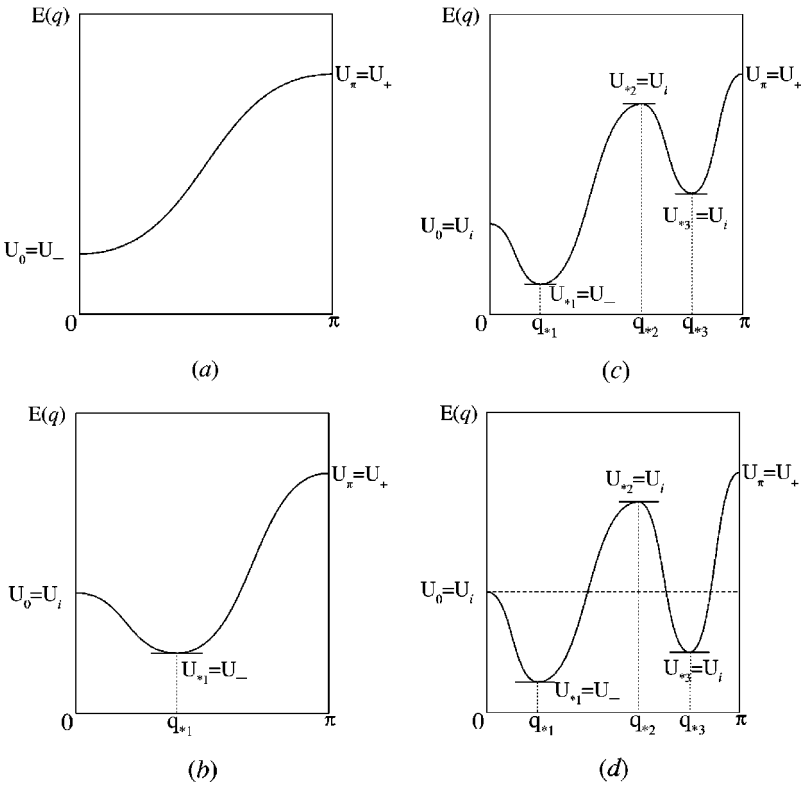

FIG. 4. The different types of energy bands possible for recursion relation (3.5) with wave function (3.8). Note $U_\pi(m)=U_+$ in all cases. (a) When $\overline{h_{xr}}<\overline{h_x}<\overline{h_{xco}}$ with $|m|<\overline{S}$ and when $\overline{h_{xc}}(m)<\overline{h_x}<\overline{h_{xr}}$ with $|m|>m_*$. In this case, $U_0(m)=U_-$, and $U_{*1}(m)$ does not appear since q_{*1} is imaginary. (b) When $\overline{h_{xc}}(m)<\overline{h_x}<\overline{h_{xr}}$ with $m_a<|m|<m_*$. Here $U_{*1}(m)=U_-, U_0(m)=U_i$. (c) When $\overline{h_{xi}}<\overline{h_x}<\overline{h_{x\,\max}}$ with $|m|<m_a$ and when $0<\overline{h_x}<\overline{h_{xi}}$ with $m_i<|m|<m_a$. (d) when $0<\overline{h_x}<\overline{h_{xi}}$ with $|m|<m_i$. Note that, in both (c) and (d), $U_{*1}(m)=U_-$, and $U_0(m), U_{*2}(m)$, and $U_{*3}(m)$ are inside the band and thus all denoted U_i.

spectively. Once this analogy is recognized, assuming $t_{m,m\pm\alpha}(\alpha=0,1,\text{ or }4)$ vary slowly with m, we can treat the recursion relation within a continuum quasiclassical approximation or a phase integral method.[21–24,27] With this approximation we can define smooth functions

$$t_\alpha(m)\simeq\frac{1}{2}(t_{m,m+\alpha}+t_{m,m-\alpha}),\quad \alpha=0,1,4. \tag{3.6}$$

For the present model, the t_α's are given by

$$t_0(m)=-m^2(1+\lambda_1 m^2),$$

$$t_1(m)=-\frac{\overline{Sh_x}}{2}\sqrt{\overline{S^2}-m^2},$$

$$t_4(m)=\lambda_2(\overline{S^2}-m^2)^2, \tag{3.7}$$

where we have used the approximation $S(S+1)\approx\overline{S^2}$. Introducing the DPI wave function within the semiclassical approximation

$$C_m\sim\frac{1}{\sqrt{v(m)}}\exp\left[i\int^m q(m')dm'\right], \tag{3.8}$$

we have the Hamilton-Jacobi equation

$$E=\mathcal{H}_{sc}(q,m)\equiv t_0(m)+2t_1(m)\cos q+2t_4(m)\cos 4q \tag{3.9}$$

and the transport equation

$$v(m)=\frac{\partial\mathcal{H}_{sc}}{\partial q}=-2\sin q(m)\times[t_1(m)+16t_4(m)\cos q(m)\cos 2q(m)]. \tag{3.10}$$

In Eqs. (3.8) and (3.10), $q(m)$ is a local, m-dependent Bloch wave vector obtained by solving Eq. (3.9) for q for any given energy E. It is very useful to have a physical picture of these equations. For a given value of m, Eq. (3.9) gives an energy band $E(q)$ which defines the classically allowed range of energies. In Fig. 4 we show possible E vs q curves for our problem. At lower and upper edges of the band the transport equation shows that $v(m)$ becomes zero because the slope $\partial E(q)/\partial q$ is zero. This means that the band edges are related to the classical turning points. These are not the only turning points, however. Such points are more generally defined by the condition that the velocity $v(m)$ vanishes. This condition produces additional loci in E-m space, which we call *critical curves*, along with the m-dependent band edges. These curves are crucial to understanding how the oscillating tunnel splitting, i.e., the quenching effect, appears.

B. Critical curves

From Eq. (3.10) the condition $v(m)=0$ is satisfied when $q=0, q=\pi$, or $q=q_*$, where q_* is the solution of

$$32t_4(m)\cos^3 q_*(m)-16t_4(m)\cos q_*(m)+t_1(m)=0. \tag{3.11}$$

Substituting these into Eq. (3.9) we obtain the following energy curves for each of the three q's:

$$U_0(m)=t_0(m)+2t_1(m)+2t_4(m),$$

$$U_{\pi}(m)=t_0(m)-2t_1(m)+2t_4(m),$$

$$U_{*}(m)=t_0(m)+2t_1(m)\cos q_{*}(m)+2t_4(m)\cos 4q_{*}(m), \tag{3.12}$$

where $U_0(m)\equiv E(0,m)$, $U_{\pi}(m)\equiv E(\pi,m)$, and $U_{*}(m)\equiv E(q_{*}(m),m)$. Whenever a given energy E crosses one of these curves a turning point occurs. Various types of turning points depending on the characteristic of the critical curves have been analyzed in Ref. 27. An interesting feature of this analysis is the existence of novel turning points inside the classically forbidden region, which is crucial for the quenching of spin tunneling. The recursion relation studied there was based on a spin Hamiltonian which includes terms up to second order, and there were only three critical curves to be considered. Here, we expect to have up to five curves, $U_0(m), U_{\pi}(m)$, and up to three $U_{*}(m)$'s from the cubic equation (3.11).

In order to proceed further, it is necessary to analyze the critical curve structure more closely, in particular its dependence on $\overline{h_x}$. To do this, let us first compare $U_0(m)$ with $U_{\pi}(m)$. From Eq. (2.7) it can be easily seen that $U_{\pi}(m)>U_0(m)$ since $t_0(m)<0, t_1(m)<0$, and $t_4(m)>0$ for all $|m|<\overline{S}$. Thus, $U_{\pi}(m)$ can be the upper band edge. However, in order for this to be so we still need to prove that $U_{\pi}(m)>U_{*}(m)$. This is not obvious. Indeed, since Eq. (3.11) is a cubic in $\cos q_{*}$, it is possible to have complex solutions. These solutions will yield a complex $U_{*}(m)$, which is not of interest because the Hamilton-Jacobi equation $E=U_{*}(m)$ cannot then be satisfied. A careful consideration of the solutions of Eq. (3.11) is therefore necessary.

Defining $x=\cos q_{*}$, $\mu=m/\overline{S}$ and using Eq. (2.7) for the t_{α}'s, we can write Eq. (3.11) as

$$f(x)\equiv 2x^3-x-\frac{\overline{h_x}}{32\lambda_2\overline{S^2}}(1-\mu^2)^{-3/2}=0. \tag{3.13}$$

A sketch of the function $f(x)$ is drawn in Fig. 5. This sketch incorporates the following easily verified properties of $f(x)$: (i) $f(0)<0$, (ii) $f'(0)=-1$, (iii) $f'(\pm 1)=5>0$, (iv) $f(-1)<0$, (v) $f(1)$ may be of either sign, and (vi) $f'(\pm 1/\sqrt{6})=0$, where $f'(x)\equiv df(x)/dx$. It follows that a curve of type marked (a), characterized by one real zero of $f(x)$, arises when $\overline{h_x}$ is large or when $|m|$ is large and that a curve of type marked (b), characterized by three real zeros, arises when $\overline{h_x}$ is small or when $|m|$ is small. Let us denote the largest zero by x_1 and the other two, when they are real, by x_2 and x_3 with $x_2>x_3$. The corresponding values for $q_{*}(m)$ and $U_{*}(m)$ are denoted by q_{*i} and $U_{*i}(m)$, with $i=1,2$, or 3. It is obvious that $x_1>0$ and that $-1<x_3<-1/\sqrt{6}<x_2<0$. The first real root yields a positive value for $\cos q_{*1}$, but since we cannot say if x_1 is greater or lesser than 1, q_{*1} may be real or purely imaginary. The other two real roots, when they exist, always yield real wave vectors q_{*2} and q_{*3}.

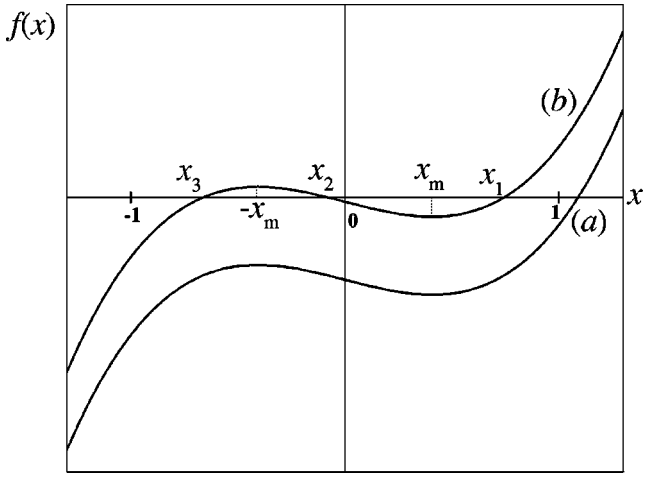

FIG. 5. Sketch of the cubic function $f(x)$ for (a) large $\overline{h_x}$, or large $|m|$, (b) small $\overline{h_x}$, or small $|m|$. Note that there is one root in (a), but three roots in (b). The transition from type (a) to type (b) occurs when $f(-x_m)=f'(-x_m)=0 (x_m=1/\sqrt{6})$, which gives the curve $\overline{h}_{xc}(m)$ in Eq. (3.14).

The transition from one to three real roots occurs when $f(x)$ has a double zero, i.e., when $f(x)$ and $f'(x)$ both vanish simultaneously. It is easily shown that this condition is equivalent to

$$\overline{h}_{xc}(m)=\overline{h}_{x\,\max}\left(1-\frac{m^2}{\overline{S^2}}\right)^{3/2}, \tag{3.14}$$

$$\overline{h}_{x\,\max}=32\sqrt{\frac{2}{27}}\lambda_2\overline{S^2}. \tag{3.15}$$

The curve $\overline{h}_{xc}(m)$ and some special values of $\overline{h_x}$ are displayed in Fig. 6. The physical meanings of these values are listed in Table I. From the arguments of the previous paragraph, it follows that we will have three zeros when $\overline{h_x}$

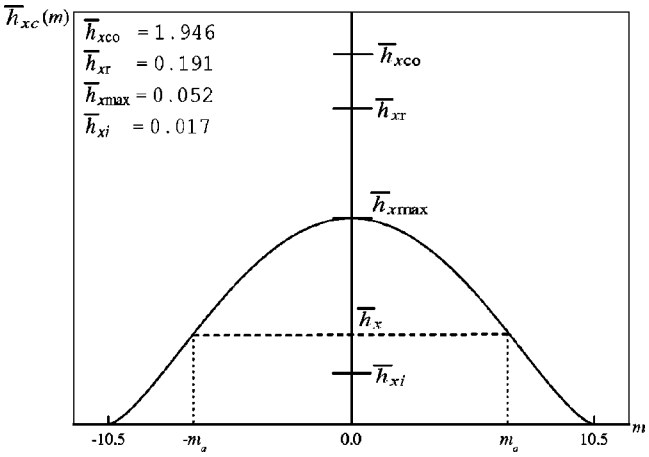

FIG. 6. The curve $\overline{h}_{xc}(m)$ and some physically meaningful values of $\overline{h_x}$'s. In the inset we list these values computed with experimental numbers for λ_1 and λ_2 for Mn_{12}-ac. Points at which $\overline{h_x}$ intersects the curve $\overline{h}_{xc}(m)$ are $m=\pm m_a$.

TABLE I. Physical meanings of the special $\bar{h}_x$'s

$\bar{h}_{xco}$	Coercive field above which no tunneling exists.
$\bar{h}_{xosc}$	The value below which the wavefunction can have an oscillating part inside the forbidden region.
$\bar{h}_{xr}$	The value above which q_{*1} becomes real.
$\bar{h}_{x\max}$	The maximum value of the curve $\bar{h}_{xc}(m)$.
$\bar{h}_{xi}$	The value at which $U_{*3}(0)$ intersects $U_0(0)$.

$<\bar{h}_{xc}(m)$ and one zero when $\bar{h}_x>\bar{h}_{xc}(m)$. When $\bar{h}_x<\bar{h}_{x\max}$, we can also ask for the points $\pm m_a(\bar{h}_x)$ at which we change from one to three real roots of $f(x)$. These are directly given by solving Eq. (3.14) for $\bar{h}_{xc}(m)=\bar{h}_x$:

$$m_a=\bar{S}\left[1-\left(\frac{\bar{h}_x}{\bar{h}_{x\max}}\right)^{2/3}\right]^{1/2}. \tag{3.16}$$

Next, let us investigate whether $U_{*1}(m)$ is inside or outside the classically allowed energy band. Since x_1 moves to larger positive values as $|m|$ increases (see Fig. 5), we see that U_{*1} lies inside the band if $x_1<1$, i.e., $|m|<m_*$, where m_* is such that $f(1)=0$. Solving this equation we get

$$m_*=\bar{S}\left[1-\left(\frac{\bar{h}_x}{\bar{h}_{xr}}\right)^{2/3}\right]^{1/2}, \tag{3.17}$$

$$\bar{h}_{xr}=\sqrt{\frac{27}{2}}\bar{h}_{x\max}. \tag{3.18}$$

Clearly, $m_a<m_*$.

Let us also explore whether the $U_{*i}(m)$'s, when they are real, are larger or smaller than $U_\pi(m)$ or $U_0(m)$. We consider the following differences:

$$U_{\pi j}(m)\equiv U_\pi(m)-U_{*j}(m)=16t_4(m)\cos q_{*j}(1+\cos q_{*j})^2 \times(-2+3\cos q_{*j}), \tag{3.19}$$

$$U_{*ij}(m)\equiv U_{*i}(m)-U_{*j}(m) =-16t_4(m)(\cos^2 q_{*i}-\cos^2 q_{*j}) \times[3(\cos^2 q_{*1}+\cos^2 q_{*j})-1], \tag{3.20}$$

$$U_{0i}(m)\equiv U_0(m)-U_{*i}(m)=16t_4(m)\cos q_{*i}(1-\cos q_{*i})^2 \times(2+3\cos q_{*i}), \tag{3.21}$$

where $i,j=1,2$, or 3 and we have used Eq. (3.11) to eliminate $t_1(m)$ in favor of $t_4(m)$. From these equations, and using the facts that $t_4(m)>0$, plus[39]

$$-\frac{1}{\sqrt{2}}\leqslant\cos q_{*3}\leqslant-\frac{1}{\sqrt{6}}\leqslant\cos q_{*2}<0, \quad \frac{1}{\sqrt{2}}\leqslant\cos q_{*1}, \tag{3.22}$$

we find the following:

(1) When there is only one real root,

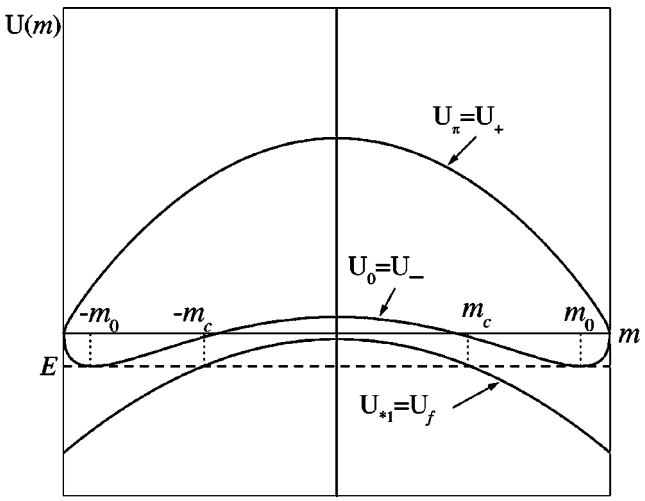

FIG. 7. The critical curves for case I. At points $\pm m_0$, U_0 has minima, and the points $\pm m_c$ denote the intersection between E and U_{*1}. Note $U_{*1}=U_f$ and $U_0=U_-$ for all $|m|\leqslant\bar{S}$. For a given value of E,q becomes complex for $|m|<m_c$ which lies inside the classically forbidden region. In this region the semiclassical wave function C_m oscillates with decaying or growing envelope.

$$U_{*1}(m)<U_0(m)<U_\pi(m) \tag{3.23}$$

for all $|m|<\bar{S}$ and $\bar{h}_{x\max}<\bar{h}_x<\bar{h}_{xco}$.

(2) When there are three real roots,

$$U_{*1}(m)<U_0(m)<U_{*3}(m)<U_{*2}(m)<U_\pi(m) \tag{3.24}$$

for $\bar{h}_{xi}<\bar{h}_x$ and

$$U_{*1}(m)<U_{*3}(m)<U_0(m)<U_{*2}(m)<U_\pi(m) \tag{3.25}$$

for $0<\bar{h}_x<\bar{h}_{xi}$, where $\bar{h}_{xi}$ is determined by $U_0(m=0,\bar{h}_{xi})=U_{*3}(m=0,\bar{h}_{xi})$, which, from Eqs. (3.21) and (3.22), is equivalent to $\cos q_{*3}(m=0,\bar{h}_{xi})=-2/3$.

We can now list the various types of critical curve patterns that arise in our problem and the corresponding ranges of the field $\bar{h}_x$. In the following, $U_-(m)$ and $U_+(m)$ denote the lower and upper bounds of the energy band, and $U_f(m)$ and $U_i(m)$ mean the forbidden and internal energies, respectively.

1. Case I: $\bar{h}_{xr}<\bar{h}_x<\bar{h}_{xco}$

In this case U_{*2} and U_{*3} are not real for any m, and $q_{*1}(m)$ is imaginary; i.e., $U_{*1}(m)$ is outside the band for all $|m|\leqslant\bar{S}$. The energy band $E(q)$ is of the type in Fig. 4(a) for all m, and the critical curves become

$$U_{*1}=U_f, \quad U_0=U_-, \quad U_\pi=U_+ \quad \text{for } |m|<\bar{S}, \tag{3.26}$$

which are shown in Fig. 7.

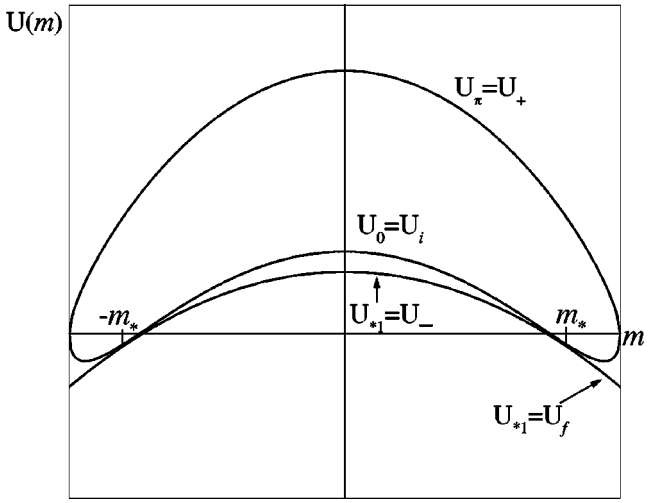

FIG. 8. The critical curves for case II. $\pm m_*$ are the points where $U_0(m)=U_{*1}(m)$ [and $dU_0(m)/dm=dU_{*1}(m)/dm$]. U_{*1} is the lower band edge in the central region $|m|<m_*$ and forbidden in the outer region $|m|>m_*$.

2. Case II: $\bar{h}_{x\max}<\bar{h}_x<\bar{h}_{xr}$

Now, U_{*2} and U_{*3} continue to be complex for all m, but $q_{*1}(m)$ is real in the central region $|m|<m_*$. In this region, the energy band is as in Fig. 4(b), while in the outer region it is of the type in Fig. 4(a). Accordingly, the critical curves have the structure shown in Fig. 8 and can be written as

$$U_{*1}=U_-,\ U_0=U_i,\ U_\pi=U_+ \quad \text{for } |m|<m_*,$$
$$U_{*1}=U_f,\ U_0=U_-,\ U_\pi=U_+ \quad \text{for } |m|>m_*. \tag{3.27}$$

3. Case III: $0<\bar{h}_x\leqslant\bar{h}_{x\max}$.

There are now three m regions. In the outer region, $|m|>m_*, U_{*2}$ and U_{*3} are still complex, U_{*1} is outside the band, and $E(q)$ has the shape in Fig. 4(a). In the intermediate range $m_a<|m|<m_*, U_{*2}$ and U_{*3} continue to be complex, but U_{*1} is inside the band and $E(q)$ has the shape in Fig. 4(b). In the central range, $|m|<m_a, U_{*2}$ and U_{*3} become real, and $E(q)$ has the shape shown in Figs. 4(c) (when $\bar{h}_{xi}<\bar{h}_x<\bar{h}_{x\max}$) and 4(d) (when $\bar{h}_x<\bar{h}_{xi}$). The critical curves can be expressed as[40]

$$U_0, U_{*2}, U_{*3}=U_i,\ U_{*1}=U_-,\ U_\pi=U_+,\ |m|<m_a,$$
$$U_0=U_i,\ U_{*1}=U_-,\ U_\pi=U_+,\ m_a<|m|<m_*, \tag{3.28}$$

which are illustrated in Figs. 9(a) and 9(b).

As a matter of fact, we should distinguish two subcases in case III. When $\bar{h}_x>\bar{h}_{xi}$, as in Eq. (3.24), the relevant critical curves are as in Fig. 9(a). When $\bar{h}_x<\bar{h}_{xi}$, as in Eq. (3.25), there is a range of m values in which $U_{*3}<U_0$ [see Fig. 9(b)]. For the experimental parameters relevant to Mn_{12}-ac, the field $\bar{h}_{xi}$ is rather small, and the points m_0, m_*, m_a, and m_i are all clustered tightly near $m=\bar{S}$. This means that for

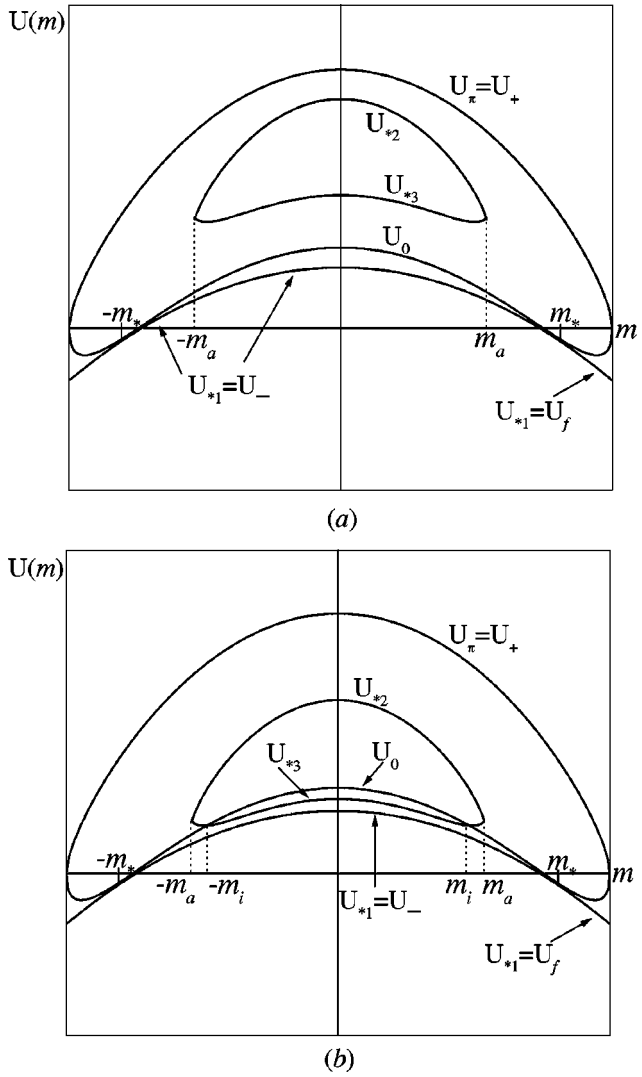

FIG. 9. The critical curves for case III. (a) When $\bar{h}_{xi}<\bar{h}_x<\bar{h}_{x\max}$ and (b) when $0<\bar{h}_x<\bar{h}_{xi}$. There are five critical curves. Note, however, that U_{*2} and U_{*3} appear only in the region $|m|<m_a$ because they are complex outside this region.

the low-lying states, there will be four turning points very close to one another, and the DPI analysis would have to be done using a *quartic* turning point formula, analogous to the quadratic turning point formula as discussed by Berry and Mount.[41] Since we know the qualitative structure of the energy spectrum for fields as small as $\bar{h}_{xi}$ from the arguments of Sec. II, this exercise is largely academic, and we have chosen not to perform it. This means that our analysis is not quite correct at very small fields, and this can be seen in Fig. 10, especially in the behavior of the splitting between the first excited pair of levels. As discussed in Sec. II, this splitting is rigorously zero at $\bar{h}_x=0$, whereas we appear to find a zero at a slightly nonzero value of $\bar{h}_x$.

As discussed in Ref. 28 the quenching of spin tunneling occurs when $q(m)$ has a real part as well as an imaginary part inside the forbidden region. From the viewpoint of energy curves this happens when there is an energy curve inside the forbidden region. From the above analysis we can

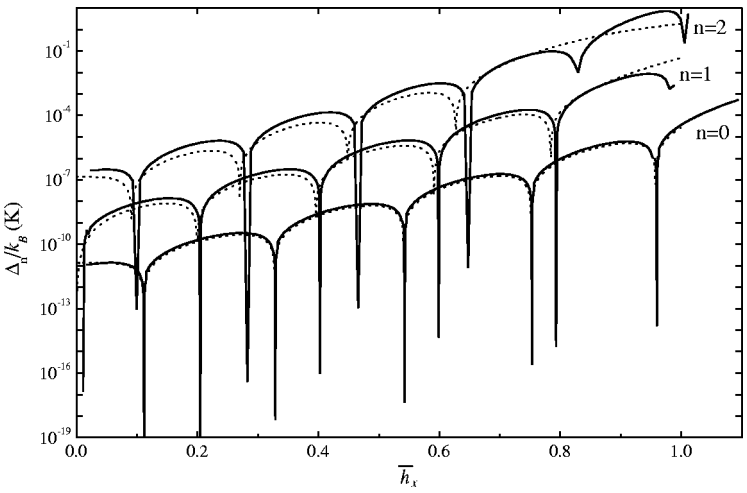

FIG. 10. Tunnel splittings Δ_n between first three pairs of levels as a function of the field parameter $\overline{h}_x$. The dotted and solid curves are obtained from exact numerical diagonalization of the Hamiltonian and the DPI method, respectively.

see that only $U_{*1}(m)$ resides inside the forbidden region. For a given energy E such that $U_{0\min} \leqslant E < U_{*1\max}$, q changes from pure imaginary to complex as m passes from the $|m| > m_c$ region to the $|m| < m_c$ region, where m_c is the point where E intersects $U_{*1}(m)$ (for example, see Fig. 7). When q becomes complex the semiclassical wave function in Eq. (3.8) oscillates with exponentially decaying or growing envelope. The quenching of spin tunneling arises from this oscillating nature of the wave fuction inside the forbidden region.

We note here that for the experimental Mn_{12} parameters, the field $\overline{h_{x\,\max}}$ is quite small (see the legend in Fig. 6), and so in the entire field range for case III, even though there is a forbidden region turning point, the behavior of the ground-state tunnel splitting is qualitatively similar to that for $\overline{h_x} = 0$. The behavior of the splitting of the next two levels is more interesting, and as can be seen from Fig. 10, the DPI method does capture it, at least qualitatively and, perhaps, even quantitatively.

C. Tunnel splittings

We now turn to calculating the energy splittings themselves. In Ref. 28, tunnel splittings for a five-term recursion relation have been obtained from Herring's formula. The final result is, however, quite general so that it can be applied to a recursion relation which includes more than five terms. Moreover, as we can notice from the above classifications, although the present nine-term case has more critical curves, the possible types of turning points are all included in those discussed in Ref. 27 and no new type of turning point emerges here. Thus, we can directly apply the formula for the tunnel splittings obtained in Ref. 28 to the present problem. Since our calculation is based on this formula we quote the main results here. The tunnel splitting for nth pair of states is given by

$$\Delta_n(\overline{h_x}) = \frac{1}{n!}\sqrt{\frac{8}{\pi}}\omega_0 F^{n+\frac{1}{2}} e^{-\Gamma_0}\cos\Lambda_n, \qquad (3.29)$$

where

$$\Gamma_0 = \int_{-m_0}^{m_0} \kappa_0(m)dm,$$

$$\Lambda_n = \int_{-m_c}^{m_c}\left(\chi_0 + \left(n+\frac{1}{2}\right)\omega_0\chi_0'\right)dm,$$

$$F = 2M\omega_0(m_0-m_c)^2 \times \exp\left(-2Q_1 + \omega_0\int_{-m_c}^{m_c}\kappa_0' dm\right),$$

$$Q_1 = \int_{-m_0}^{-m_c}\left(\frac{\omega_0 B_0'}{\sqrt{B_0^2-1}} + \frac{1}{m+m_0}\right)dm. \qquad (3.30)$$

Here, κ and χ are the imaginary and real parts of complex q, respectively, and

$$\kappa_0 = \kappa(m,\epsilon=0), \quad \kappa_0' = \left.\frac{\partial\kappa(m,\epsilon)}{\partial\epsilon}\right|_{\epsilon=0},$$

$$\chi_0 = \chi(m,\epsilon=0), \quad \chi_0' = \left.\frac{\partial\chi(m,\epsilon)}{\partial\epsilon}\right|_{\epsilon=0},$$

$$B_0 = \cos q(m,\epsilon=0), \quad B_0' = \left.\frac{\partial\cos q(m,\epsilon)}{\partial\epsilon}\right|_{\epsilon=0}, \qquad (3.31)$$

with $\epsilon \equiv E - U_-(-m_0)$. In these equations, $\pm m_c$ are not quite the turning points of the previous subsection, in that they are not the point where $U_{*1}(m)$ equals the true energy E_n of the nth pair of levels. Rather, they are the points where $U_{*1}(m) = U_-(\pm m_0)$, which corresponds to setting $E = U_-(m_0)$, i.e., $\epsilon = 0$. The reason is that the formula (3.29) incorporates expansions of various phase integrals in the energy difference

$$\epsilon_n = E_n - U_-(m_0) = \left(n+\frac{1}{2}\right)\omega_0, \qquad (3.32)$$

which is of order $(1/S)$ compared to the energy barrier, as long as $n \ll S$. This is why m_c is modified and also why the primary phase integral for the Gamow factor Γ_0 runs from

$-m_0$ to m_0, the minima of $U_0(m)$, rather than between the points where $U_0(m)=E_n$. Since all energy curves are a function of both m and $\overline{h_x}$, these points still depend on $\overline{h_x}$, which in turn makes the Δ_n depend on $\overline{h_x}$.

The mass M and frequency ω_0 in Eq. (3.30) are obtained by approximating $U_-(m)$ near its minima by a parabola, i.e., $U_-(m)=E+\frac{1}{2}M\omega_0^2(m\pm m_0)^2$. We find

$$M=-\frac{1}{2t_1(-m_0)+32t_4(-m_0)},$$

$$\omega_0^2=-2[t_1(-m_0)+16t_4(-m_0)]\left.\frac{\partial^2 U_-}{\partial m^2}\right|_{m=-m_0}. \tag{3.33}$$

The application of formulas (3.29)–(3.33) cannot be carried out in closed form all the way, and we must resort to numerical methods. We explain the principal steps in our numerical calculation below.

In step 1, we must find $\pm m_0$ and $U_-(\pm m_0)$. For our problem we discover that $U_-(m)$ is always given by $U_0(m)$ near the classically allowed minima. The equation for the minima can be reduced to another cubic

$$\overline{S^2}\overline{h_x^2}=4(\overline{S^2}-y)[2(\lambda_1-2\lambda_2)y+1+4\lambda_2\overline{S^2}]^2, \tag{3.34}$$

where $y=m^2$. For the parameters λ_1 and λ_2 of interest to Mn_{12} and $\overline{h_x}<\overline{h_{xco}}$, all three roots of this cubic equation are real, but only one is positive. This root gives us m_0, and substitution of this value into Eq. (3.12) for $U_0(m)$ gives E, and Eqs. (3.33) then give M and ω_0.

Step 2 is to obtain the points $\pm m_c$ given by the roots of the equation

$$U_{*1}(m)=U_-(m_0). \tag{3.35}$$

As discussed after Eq. (3.32), up to terms of relative order $(1/S)$, the points $\pm m_c$ are the actual turning points for the low-lying energies. Note that it is U_{*1} which appears in Eq. (3.35) since this is the critical curve that lies in the classically forbidden region.

To solve Eq. (3.35) numerically, we first solve Eq. (3.11) for the function $\cos q_{*1}(m)$, which can be done in closed form. This solution is then substituted in Eq. (3.12) to obtain $U_{*1}(m)$. The entire procedure can be implicitly implemented in the numerical routine. The same holds for $dU_{*1}(m)/dm$. Since $U_-(m_0)$ is known from step 1, any of the standard root-finding methods—Newton-Raphson, bisection, secant, etc.—can be applied to Eq. (3.35).

Step 3 is to find $q(m)$, in particular its real and imaginary parts $\kappa_0(m)$ and $\chi_0(m)$. This is done by solving the Hamilton-Jacobi equation (3.9) with the energy E found in the first step. The problem amounts to solving a quartic equation in $\cos q$ and making sure that one has the correct solution, which can be done easily by making use of the properties that we have found above. Thus, in the region $m_c<|m|<m_0$, there are two solutions of the form $i\kappa$ (with κ real) and two of the form $\pi-i\kappa$. We discard the latter and of the former select that one which continuously tends to 0 as $m\to\pm m_0$. In the region $|m|<m_c$, the solutions can be written as $i\kappa\pm\chi$ and as $\pi-(i\kappa\pm\chi)$, where $\chi\to 0$ as $m\to\pm m_c$. We discard the latter two and read off $\kappa(\equiv\kappa_0)$ and $\chi(\equiv\chi_0)$ from the imaginary and real parts of the first two. Note that both κ_0 and χ_0 are taken to be positive.

Step 4 is to find the ϵ partial derivatives κ_0' and χ_0', in effect $\partial q(\epsilon,m)/\partial\epsilon$. ($B_0'$ is directly obtainable from κ_0'.) We differentiate the Hamilton-Jacobi equation with respect to E:

$$-2[t_1\sin q+4t_4\sin 4q]\frac{\partial q}{\partial\epsilon}=1. \tag{3.36}$$

Since $q(m)$ is found in step 3, this equation gives $\partial q/\partial\epsilon$ for any m directly.

We now have all the ingredients needed to evaluate the one-dimensional integrals Γ_0,Λ_n,F, and Q_1. This is a straightforward numerical procedure. The only point worth noting is that the integrand for Q_1 is nonsingular at $m=-m_0$ and behaves, in fact, as $(m+m_0)$.

In Fig. 10 we show the tunnel splittings for first three pairs of states as a function of the field parameter $\overline{h_x}$. For comparison we also plotted the tunnel splittings obtained from exact diagonalization of the Hamiltonian.

From the results we observe several interesting features. First, as anticipated, the tunnel splittings are completely suppressed at certain values of H_x. A large part of the overall pattern of zeros, their number, and the dependence of this number on n, the pair index, etc., has already been discussed qualitatively in Sec. II. What is surprising is how regularly spaced the diabolical values of H_x are. For the first pair of splittings, e.g., the intervals between successive zeros decrease by 2% or 3% only and the last interval is 92% of the first. For the next pair Δ_2, the last interval is 95% of the first. The mean interval between zeros for the first three pairs is $\Delta H_0\simeq 0.93$ T, $\Delta H_1\simeq 0.85$ T, and $\Delta H_0\simeq 0.79$ T.

The regularity of the zeros means that the phase integral Λ_n decreases almost linearly with $\overline{h_x}$. (From Fig. 10, the Gamow factor Γ_0 also appears to be quite linear in $\overline{h_x}$.) While this variation is clearly expected to be smooth, we have no *a priori* way to judge how linear it will be. A similarly strong regularity of quenching intervals is experimentally seen in Fe_8. The simplest model Hamiltonian for Fe_8 entails only second-order terms in the components of the spin operator, and in this model, the spacing of zeros *is* exactly equal,[20] but to describe actual Fe_8, one must add fourth-order terms. These terms change the spacing significantly, but still seem to preserve its regularity. It would be interesting to find a physical argument for this feature, which appears to be somewhat general.

IV. PERTURBATIVE CALCULATION

For the purposes of this section, it is useful to review some basic facts pertaining to degeneracy in quantum mechanics in the absence of symmetry. As a rule, eigenvalues of a finite Hamiltonian are all simple. For a general Hamiltonian, represented by a complex Hermitian matrix we must be able to adjust at least three parameters in order to produce

a degeneracy. An approximate physical argument is as follows.[42] Let two states m and m' be approximately degenerate and write the secular matrix between them as

$$\begin{pmatrix} E_m & V_{mm'} \\ V_{m'm} & E_{m'} \end{pmatrix}, \tag{4.1}$$

with $V_{m'm}=V_{mm'}^*$. The states will be truly degenerate only if the following two conditions are met:

$$B_{mm'} \equiv E_m - E_{m'} = 0, \tag{4.2}$$

$$V_{mm'} = 0. \tag{4.3}$$

We shall refer to these as the no-bias and no-mixing conditions, respectively.[29] Since $V_{mm'}$ is in general complex, we have three real conditions requiring three or more variable parameters for their satisfaction.

Precisely three parameters are available to us in Eq. (1.2) in the three components of **H**. If the Hamiltonian matrix is real symmetric, the number of adjustable parameters required is lowered to 2. In the present problem, this situation is realized when $H_y=0$, and so, as for Fe_8, we expect to find degeneracies in the H_x-H_z plane. Unless explicitly stated, we will henceforth take $H_y=0$, so that $V_{mm'}=V_{m'm}$.

Ignoring an additive constant, the energy surface in the vicinity of the degeneracy is given by

$$E = \pm (B_{mm'}^2 + V_{mm'}^2)^{1/2}, \tag{4.4}$$

which has the form of a double cone or a *diabolo* in H_x-H_z space.

Let us first take $H_x=0$, i.e., $\mathbf{H} \| \hat{\mathbf{z}}$. As argued in Sec. II, levels belonging to different subspaces can cross. The fields at which they do so can be approximately found by neglecting the $S_\pm^4$ terms. The crossing conditions are $E_m=E_{m'}$, where $E_m=-Am^2-Bm^4-g\mu_B H_z m$. Improved formulas can be obtained by finding corrections to E_m perturbatively in C. These intersections are easy to understand in terms of symmetry (invariance of $\mathcal{H}$ under a rotation by 90° about $\hat{\mathbf{z}}$).

If H_x and H_z are both nonzero, there is no obvious symmetry. If H_x and C are both small, however, we may continue to label the states by the m quantum numbers and calculate the energies perturbatively in these two parameters. In terms of the secular matrix (4.1), the energies E_m and $E_{m'}$ and the bias $B_{mm'}$ are determined by the terms in S_z in Eq. (1.2) and the mixing $V_{mm'}$ by the terms involving C and H_x. The energies are trivial to find, so the problem is to find $V_{mm'}$.

As in Sec. III, it is convenient to divide $\mathcal{H}$ by A and to work with scaled quantities $\lambda_1=B/A$ and $\lambda_2=C/A$. However, we scale the magnetic fields slightly differently:

$$h_{x,z} = H_{x,z}/SH_c. \tag{4.5}$$

As before, $H_c \equiv A/g\mu_B$.

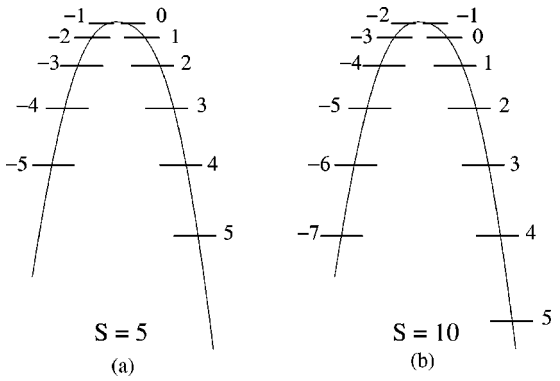

FIG. 11. (a) Energy level diagram for $S=5$, with $B=0$, and $h_z=1/5$. (b) Part of diagram for $S=10$ with $h_z=0.3$, showing that the pattern above any two degenerate levels depends only on Δm, irrespective of S.

A. Simplified model: $B=0$

To keep the problem tractable, let us set $B=0$ at this stage. Then, to zeroth order in both C and H_x, $E_m=-Am^2-g\mu_B H_z m$. Hence, levels m and m' are degenerate when

$$h_z = -\frac{m+m'}{S}. \tag{4.6}$$

It remains to find the off-diagonal element $V_{mm'}$. As we shall see, the choice $B=0$ simplifies the calculation greatly, for E_m is then quadratic in m, and energy level differences are linear in m and given by a fixed set of numbers whenever Eq. (4.6) holds.

To illustrate the calculation of $V_{mm'}$, we consider the case $S=5$. Suppose $h_z=1/5$, so that $m=-5$ and $m'=4$ are degenerate (see Fig. 11). We will find $V_{4,-5}$ to leading nonzero order in h_x and C as a double series in these variables. It is clear that a transition from m to m' can be made in three ways: (1) act with $h_x S_+$ in ninth order, (2) act with $h_x S_+$ in fifth order and CS_+^4 in first order, and (3) act with $h_x S_+$ in first order and CS_+^4 in second order.

We denote the corresponding contributions to V by $V^{(1)}, V^{(2)}$, and $V^{(3)}$. Each of these involves a product of matrix elements and a product of energy denominators. For $V^{(1)}$, the former is

$$\frac{1}{2^9}\langle 5,4|S_+^9|5,-5\rangle(-h_x S)^9 \equiv W(-h_x S)^9, \tag{4.7}$$

where $W=709\sqrt{10}$. The energy denominators can be read off Fig. 11(a). For $V^{(1)}$, the net denominator is

$$(-1)^8(8\times 14\times 18\times 20)^2 \equiv (-1)^8 K^2. \tag{4.8}$$

The factor $(-1)^8$ appears here because all intermediate states are higher in energy than E_{-5} and E_4. Putting together Eqs. (4.7) and (4.8), we get

$$V^{(1)} = -\frac{W}{K^2}(h_x S)^9. \tag{4.9}$$

TABLE II. Transition paths and energy denominators for perturbative calculation of $V^{(2)}$.

Transition path	Energy denominator product
$-5\rightarrow-1\rightarrow0\rightarrow1\rightarrow2\rightarrow3\rightarrow4$	$(-1)^5 20K$
$-5\rightarrow-4\rightarrow0\rightarrow1\rightarrow2\rightarrow3\rightarrow4$	$(-1)^5 8K$
$-5\rightarrow-4\rightarrow-3\rightarrow1\rightarrow2\rightarrow3\rightarrow4$	$(-1)^5(8\times14/20)K$
$-5\rightarrow-4\rightarrow-3\rightarrow-2\rightarrow2\rightarrow3\rightarrow4$	$(-1)^5(8\times14/20)K$
$-5\rightarrow-4\rightarrow-3\rightarrow-2\rightarrow-1\rightarrow3\rightarrow4$	$(-1)^5 8K$
$-5\rightarrow-4\rightarrow-3\rightarrow-2\rightarrow-1\rightarrow0\rightarrow4$	$(-1)^5 20K$

For $V^{(2)}$, the transition can occur in a total of six ways, corresponding to where the S_+^4 term acts (see Table II). The product of matrix elements in each case is

$$\left(-\frac{h_x S}{2}\right)^5 \lambda_2 \langle 4|S_+^9|-5\rangle = -2^4 W \lambda_2 (h_x S)^5. \quad (4.10)$$

The energy denominators, however, depend on the transition path and are listed in Table II. Adding together all the contributions, we get

$$V^{(2)} = \frac{2^4\times 99}{140}\frac{W}{K}(h_x S)^5 \lambda_2. \quad (4.11)$$

Last, for $V^{(3)}$, there are three transition paths (i) $-5\rightarrow-1\rightarrow3\rightarrow4$, (ii) $-5\rightarrow-1\rightarrow0\rightarrow4$, and (iii) $-5\rightarrow-4\rightarrow0\rightarrow4$. The transition element product for all three is $-2^8 W(h_x S)\lambda_2^2$, and the energy denominator product is $20\times8, 20\times20$, and 8×20, respectively. Thus,

$$V^{(3)} = -\frac{2^8\times3}{200} W(h_x S)\lambda_2^2. \quad (4.12)$$

Adding together $V^{(1)}, V^{(2)}$, and $V^{(3)}$, we obtain the net $V_{4,-5}$ (restoring the level quantum numbers). For a diabolical point, this quantity should vanish. In addition to $h_x=0$, this happens when

$$\xi^2 - \frac{99K}{140}\xi + \frac{3K^2}{200} = 0, \quad (4.13)$$

where $\xi=\lambda_2^{-1}(Sh_x/2)^4$. Solving this equation and using the scaled value $\lambda_2 = 2.16\times10^{-4}$ for $S=5$, we obtain $h_x = 0.2643$ and 0.6252, while direct numerical diagonalization yields $h_x = 0.2669$ and 0.638.

Readers will undoubtedly have noted that apart from an overall factor of h_x to some power, our perturbation method yields the off-diagonal element as a homogeneous polynomial in h_x^4 and λ_2. It is not difficult to see that this will be generally true and also not difficult to justify. Let us first take the point that we have only included transition paths that go through the higher-energy levels. Consider, e.g., the path for $V_{4,-5}$ in the above calculation that goes from -5 to $+1$ via six successive $h_x S_+$ terms, then to $+5$ via a CS_+^4 term, and finally to $+4$ via an $h_x S_-$ term. This term is of order $h_x^7\lambda_2$ and should be regarded as a higher-order correction to $V^{(2)}$. Second, it is positive and of the same sign as $V^{(2)}$, because it involves six negative and one positive energy denominators. This feature is also generally valid and is important in light of the next point, which is that the sign of the terms in the polynomial for the off-diagonal element alternate when organized as a series in λ_2. Thus, for $V_{4,-5}, V^{(1)}$ is negative, $V^{(2)}$ is positive and $V^{(3)}$ is negative. This is a consequence of the fact that replacing four $-h_x S_+$ terms by a single CS_+^4 term (*a*) leaves the sign of the matrix element product unchanged, but (*b*) replaces four negative energy denominators by a single negative one.

Let us call the polynomial that remains after we have canceled off as many overall factors of $h_x S$ from $V_{mm'}$ as possible the *underlying polynomial*. It is clear that this polynomial is of degree

$$n_{mm'} = \left[\left|\frac{m-m'}{4}\right|\right] \quad (4.14)$$

in h_x^4, where $[x]$ denotes the integer part of x, i.e., the largest integer less than or equal to x. The alternation of signs of successive powers of h_x^4 is a necessary (but not sufficient) condition for all $n_{mm'}$ roots to be positive.[43] This means that, not including the points on the h_x or h_z axes, it is possible for states labeled by m and m' to intersect in a diabolical point *up to* $n_{mm'}$ times in the first quadrant of the h_x-h_z plane. This appears to us to be a topological property of the Mn_{12} Hamiltonian that is not altered by presence of higher-order terms, as long as the symmetry is not changed. Of course, the number of diabolical points may be smaller, but we do not believe it can be greater, because if h_x is sufficiently large, the term $H_x S_x$ dominates the energy in the equatorial plane, and the possibility of interfering trajectories is lost. We do not have a proof of these statements, which must be regarded as conjectures, but the similarity to Fe_8 and all the empirical evidence we have gathered suggests that they are indeed true.

For $S=5$, we have found all the diabolical points using this perturbation approach and also numerically. In all cases, the perturbative answers are nearly exact. The results are shown in Fig. 12.

At this point we wish to note a remarkable feature of this approximation, which may have been noticed by some readers. This is that the diabolical values of h_x depend on m and m' only through the combination $\Delta m = m' - m$. This means that in Fig. 12, the theoretical points corresponding to the same value of Δm are vertically aligned. See, for example, the points with $(m,m')=(-4,4)$ and $(-5,3)$, or the points with $(m,m')=(-5,2)$ and $(-4,3)$. The reason is that when we set $B=0$, the energy E_m is a quadratic function of m, and when levels m and $m'>m$ are degenerate,

$$E_{m+k} - E_m = k(\Delta m - k). \quad (4.15)$$

Thus, *the entire pattern of energy levels above the levels m* and m' *depends only on* Δm (see Fig. 11), and since only these levels enter into our perturbation theory, the energy denominators are identical. The matrix elements are of course different, but since our transition paths involve no closed loops, they amount to a net factor of $\langle m'|S_+^{\Delta m}|m\rangle$ in each term, which drops out of the underlying polynomial. In short, the entire polynomial depends only on Δm.

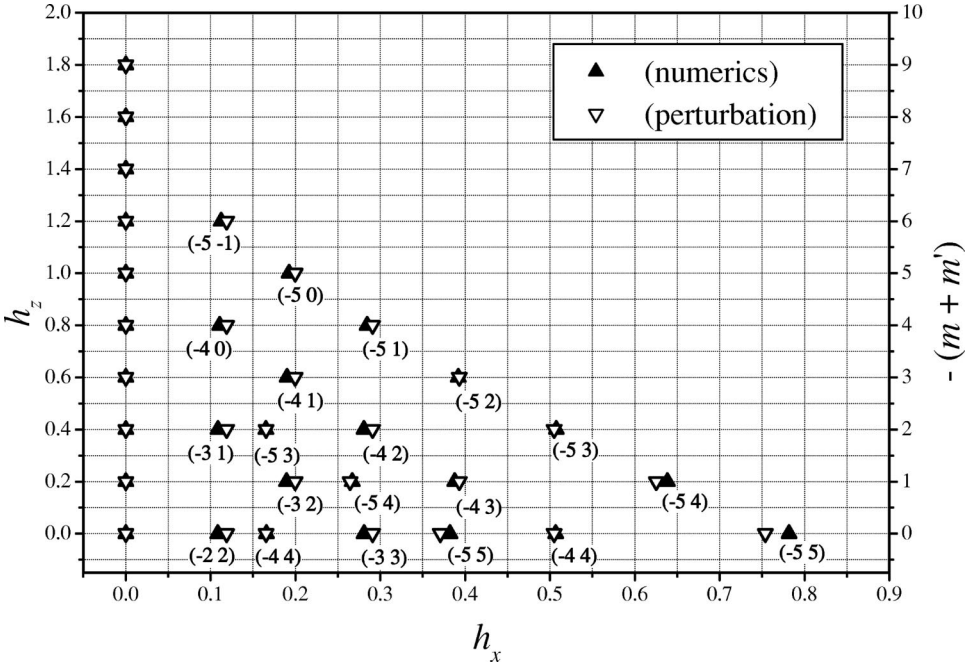

FIG. 12. Diabolical points for $S=5$. For λ_2 we have used the scaled value 2.16×10^{-4}. Each point is labeled by the Zeeman quantum numbers (m,m') except those on the h_z axis. Note that points with the same value of $m+m'$ are horizontally aligned, while those with the same $\Delta m=m'-m$ are vertically aligned. For the points on the h_z axis, any pair (m,m') is allowed, consistent with the given value of $m+m'$ and the rule $\Delta m\neq 4n$.

Furthermore, we see from Eq. (4.15) that value of S also does not enter in the energy denominators. This means that the polynomials found for $S=5$ are applicable to the $S=10$ problem for transitions with $\Delta m\leqslant 10$ and makes it worthwhile to find all the remaining polynomials for $S=10$. The task is easily automated on a computer. As an example, the polynomial for $\Delta m=13$ is

$$\xi^3-286g\xi^2+9767g^2\xi-11\,858g^3, \tag{4.16}$$

where $\xi=\lambda_2^{-1}(Sh_x/2)^4$ and $g=1440$. The full list of polynomials is given in Table I of the EPAPS depository, along with the roots for h_x for general S and λ_2, as well as for the values applicable to Mn_{12}-ac.[36]

One last general point worth noting is that for a diabolical point labeled by the pair (m,m') with $m'>m$, the energy levels which are degenerate are numbers $2S+(m-m')+1$ and $2S+(m-m')+2$, where the ground state is given the number 1.

B. Inclusion of S_z^4 term

When we try and compare the results of the previous subsection with numerics on Eq. (1.2) with $B\neq 0$, we find that the systematics of the diabolical points are fully captured in that the analytic results provide a complete indexing scheme, but the error for Mn_{12}-ac is as bad as 30% in some cases. We therefore seek some way to incorporate the $B\neq 0$ effects.

It is easy to include B in the no-bias condition. Equation (4.6) is modified to

$$h_z(m,m')=-\frac{1}{S}(m+m')[1+\lambda_1(m^2+m'^2)]. \tag{4.17}$$

The no-mixing condition is harder to evaluate. A simple minded approach is to shift the energy levels so as to retain the same relative spacings as when $B=0$, but allow the overall range to be modified.

With this in mind, let us first consider the energies when $\lambda_1=0$. When levels m and m' are degenerate, the level at the top of the barrier is given by the quantum number $k=(m+m')/2$, whenever this is an integer, or by the nearest two integers if it is a half-integer. In the spirit of our approximations, keeping track of this distinction would be an overrefinement, so we will use the formula $(m+m')/2$ in both cases. The energy range is thus given by

$$\Delta E^{(0)}=E_k^{(0)}-E_m^{(0)}=\frac{1}{4}(m-m')^2, \tag{4.18}$$

where the (0) superscript indicates that $B=0$. With $B\neq 0$, we get

$$\Delta E^{(1)}=\Delta E^{(0)}-\lambda_1\left[\left(\frac{m+m'}{2}\right)^4-m^4\right]+\lambda_1(m+m')\times(m^2+m'^2)\left[\frac{m+m'}{2}-m\right]=\gamma_{mm'}\Delta E^{(0)}, \tag{4.19}$$

where

$$\gamma_{mm'}=1+\frac{\lambda_1}{4}(7m^2+10mm'+7m'^2). \tag{4.20}$$

If we assume that the entire spectrum gets modified from its quadratic form by a uniform stretching factor $\gamma_{mm'}$, then the only change in our perturbation theory is that all energy denominators get multiplied by this factor. In the underlying

polynomial, h_x and λ_2 get replaced by $h_x/\gamma_{mm'}$ and $\lambda_2/\gamma_{mm'}$, and hence the no-mixing condition becomes

$$h_x(m,m') = \gamma_{mm'}^{3/4} r_\alpha(\Delta m), \quad \alpha = 1,2,\ldots,n_{mm'}, \tag{4.21}$$

where $\{r_\alpha\}$ are the original h_x values obtained from the roots of the underlying polynomial $P_{\Delta m}$.

The formulas (4.17) and (4.21) are compared with exact numerical results in Table II of the EPAPS depository.[36] The errors are now typically about 10% and can be of either sign.

It is useful to briefly discuss our numerical procedure. For points lying on the H_z or H_x axis, the splitting is a function of one variable, and its zeros can be found by simple scanning. For the off-axis zeros, this is harder, and we resort to the Herzberg and Longuet-Higgins sign change theorem,[11,44] which applied to the present problem states that, upon adiabatic traversal of a closed contour in the H_x-H_z plane enclosing a single point of degeneracy of two states, the wave function of either of these two states returns to itself except for a change in sign. Conversely, there is no change in sign if the contour does not enclose a degeneracy. Hence, to find a diabolical point, we first find a sign-reversing rectangular contour by hit and trial. By bisecting this rectangle in the x and z directions alternately and using the sign-change test at each bisection, we can corral the degeneracy to the degree desired. We have found this procedure to be generally superior to a direct minimization of the energy difference for the reason that the diabolo in the vicinity of a degeneracy is highly asymmetrical in the x and z directions. Consider, for example, the fourth and fifth energy levels from the bottom when $h_z \simeq 0.12$–0.13, corresponding approximately to the m quantum numbers -9 and 8. Since these states are separated by a high barrier, the mixing element between them is best understood as arising from tunneling and will therefore contain an exponentially small Gamow factor $e^{-\Gamma}$, where Γ is a tunneling action. Thus the energy surface consists of a deep and narrow valley running nearly parallel to the h_x axis, with a valley floor that goes to zero linearly at occasional points and may rise and fall in between. Because of this shape and because the surface is not analytic in the vicinity of the points being sought, standard methods for finding the minima of a function are often not well suited.

The above argument also enables us to understand an observation made by Berry and Wilkinson[11] and Berry and Mondragon[45] in the study of two very different model problems, namely, that the energy cone near a diabolical point has very high eccentricity in terms of the physically natural parameters describing the system. In other words, the cross section of the energy surface is a very long and narrow ellipse in one direction. Let us see how this happens in the present problem. To save writing let us write just x and z for the deviations of h_x and h_z from a diabolical point at (h_{x0}, h_{z0}). In the vicinity of this point, we have

$$B_{mm'} \simeq az, \tag{4.22}$$

$$V_{mm'} \simeq be^{-\Gamma}x, \tag{4.23}$$

where a and b are constants of order unity. Thus the energy surface is

$$E \simeq (a^2z^2 + b^2e^{-2\Gamma}x^2)^{1/2}. \tag{4.24}$$

The cross section is an ellipse with major axis parallel to x and eccentricity $\sim e^{\Gamma} \gg 1$. This scenario is expected to be quite general. The no-bias condition defines a line in parameter space. The gradient of the bias normal to this line is generally expected to be of order unity in the natural physical variables. The mixing element also varies on the same order unity scale in the parameter space, but because it arises from tunneling, its absolute scale is very small. The result is an energy surface of high eccentricity of the type just described.

C. Merged diabolical points

Our discussion of diabolical points[46] needs some elaboration for certain degeneracies lying on the h_z axis. For the pair $(m,m') = (-10,9)$, e.g. (more generally any pair with $\Delta m = 4n+3$), we peeled off a factor of h_x^3 from the mixing element. Writing $x = h_x$ and $z = h_z$ as in Eq. (4.24) and $z_0 = h_{z0}$ for the point of degeneracy, the bias and mixing are given by

$$B_{mm'} \approx z - z_0, \tag{4.25}$$

$$V_{mm'} \approx x^3 + O(x^7), \tag{4.26}$$

ignoring multiplicative constants. Correspondingly, the energy surface is $[(z-z_0)^2 + x^6]^{1/2}$, whose cross section is no longer an ellipse. There is also no reason for the simple sign-change result to hold *a priori*.

These conclusions are based on perturbation theory, however. More generally, we can only argue on grounds of symmetry that, under $x \to -x$, $B_{mm'} \to B_{mm'}$ and $V_{mm'} \to \pm V_{mm'}$. Instead of Eqs. (4.25) and (4.26), we should therefore expect the general expansion to take the form

$$B_{mm'} \approx z - z_0 + ax^2 + O((z-z_0)^2, x^2(z-z_0)^2, x^4), \tag{4.27}$$

$$V_{mm'} \approx x^3 - bx + cx(z-z_0) + O(x^3(z-z_0), x^5), \tag{4.28}$$

where a, b, and c are constants, all of which we expect to be very small on account of the quantitative accuracy of the perturbative approach. Ignoring the higher-order terms, the bias vanishes on the parabola $z = z_0 - ax^2$. On this parabola, the mixing is given by

$$(1-ac)x^3 - bx, \tag{4.29}$$

which vanishes at $x = 0$ and $x = \pm[b/(1-ac)]^{1/2} \equiv \pm x_1$, assuming that $b/(1-ac) > 0$. Thus, instead of a single degeneracy at $(0,z_0)$, we have three closely spaced degeneracies at

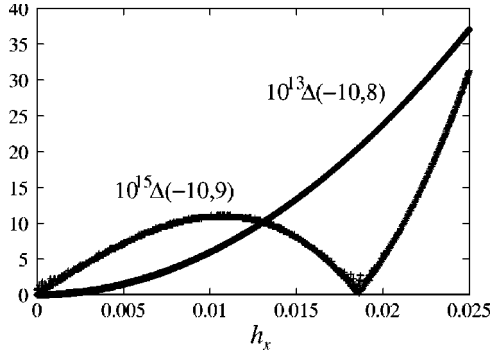

FIG. 13. Merged and nearly merged diabolical points. The plot shows the tunnel splitting $\Delta(m,m')$, showing how the triply merged $[(m,m')=(-10,9)]$ point is split, but the doubly merged $[(m,m')=(-10,8)]$ point is not. The splitting is calculated along the bottom of the parabolic trench in the h_x-h_z plane. In other words, for each value of h_x, what is plotted is the minimum of the splitting with respect to h_z. For the $-10\leftrightarrow 9$ triple merger, the points are very well fit by the curve $\Delta=|\alpha h_x(1-h_x^2/h_{x1}^2)|$, with $\alpha=1.51\times 10^{-12}$ and $h_{x1}=0.018\,55$. Indeed, the curve cannot be distinguished from the points on the scale of the figure. Similarly, the $-10\leftrightarrow 8$ splitting is very accurately fit to a parabola.

$$(0,z_0), \quad (\pm x_1, z_0 - a x_1^2). \tag{4.30}$$

The energy surface in the immediate vicinity of each one of these points is now diabolical in the ordinary sense. A small circuit of each of these points separately will therefore lead to a sign reversal, as will a larger circuit enclosing all three of them. If we ignore the splitting, we may regard the original degeneracy on the h_z axis as a *triply merged* diabolical point.

It is useful to think of the coefficients a, b, and c as depending on parameters in the Hamiltonian other than the components of **H**, e.g., λ_1 and λ_2. It may be that as these parameters are varied, the quantity $b/(1-ac)$ becomes negative, so that the roots $\pm x_1$ cease to be real. We can think of the two off-axis diabolical points as having annihilated each other, leaving behind only one true diabolical point on the axis. Unless one is very close to this point, however, the energy surface may still resemble that of a triply merged point.

For the parameters appropriate to Mn_{12}-ac, we find that the points are located at[47]

$$(h_x,h_z)=(0.0,\,0.135\,836\,224),$$
$$(\pm 0.018\,55,\,0.135\,832\,551). \tag{4.31}$$

These numbers are obtained by using the same sign-reversal theorem as previously described. Because the energy difference depends so sensitively on h_z, however, we have confirmed them in another way. For any given value of h_x, we first find the minimum of the relevant energy gap Δ with respect to h_z. In essence, we find the value of the gap at the bottom of the parabolic trench where the bias vanishes. A plot of this gap versus h_x should be given by the absolute value of the expression (4.29). As shown in Fig. 13, this is indeed so, and the split off point is again found to be at $h_x=0.018\,55$.

In exactly the same way, we may also consider *doubly merged* points, corresponding to the tunneling of states with $\Delta m=4n+2$, e.g., $(m,m')=(-10,8)$, when $h_x\approx 0$. We can continue to expand the bias as in Eq. (4.27), but the leading term in $V_{mm'}$ is now proportional to x^2, so that instead of Eq. (4.28), we have

$$V_{mm'}\approx x^2+O((z-z_0),x^2(z-z_0),x^4). \tag{4.32}$$

It is then obvious that the double zero of $V_{mm'}$ at $x=0$ cannot be split. This conclusion can also be reached in another way. Symmetry would require that, if they split, the points be located at $(\pm x_0,z_0)$, with $x_0\neq 0$. The selection rule argument given in Sec. II shows, however, that this is impossible, as there must be a crossing of any two levels m and m' with $\Delta m\neq 4n$ as H_z is varied with $H_x=0$. In Fig. 13, we also show the $(m,m')=(-10,8)$ gap at the bottom of the no-bias trench. It is apparent that now the diabolical points remain unsplit at $h_x=0$, and the curve is extremely well fit by a parabola, as required by Eq. (4.32). The merged point itself is at $h_x=0$, $h_z=0.264\,938\,170\,04$, which we find by minimizing the energy splitting, the sign-change test being useless.

Finally, the points on the h_z axis, corresponding to $\Delta m=4n+1$ are singly diabolical to begin with, so the issue of splitting does not arise.

V. SUMMARY

In this paper, we have used the DPI method and perturbation theory to study tunneling in fourfold-symmetric magnetic molecules, such as Mn_{12}, especially its behavior in a magnetic field, which is expected to show oscillations and diabolical points as in Fe_8. The DPI recursion relation now has nine terms, complicating the analysis. There may be up to five critical curves, which leads to many more turning points. The method still works, however, even though the phase integrals and integrands must be evaluated numerically. But the numerical procedures required are simple and involve only root finding and integration in one variable. Except for some special narrow-field regions, where two or more turning points merge, the DPI analysis based on linear turning point formulas is extremely good and agrees with exact numerical results quantitatively. A perturbation theory in the parameters H_x and C is found to give a very good qualitative and even quantitative understanding. Our central results are formulas (4.17) and (4.21), which along with the results in Table I of Ref. 36 give the full set of diabolical points for any molecule with $S\leqslant 10$.

ACKNOWLEDGMENTS

We are indebted to Wolfgang Wernsdorfer for very useful correspondence. C.-S.P.'s reserach was supported by the research fund of Dankook University in 2000, and A.G.'s research was partly supported by the NSF via Grant No. DMR-9616749.

*Permanent address: Department of Physics, Dankook University, Cheonan, 330-714, Korea.
Electronic address: pacs@anseo.dankook.ac.kr
†Electronic address: agarg@northwestern.edu

[1] *Quantum Tunneling of Magnetization—QTM'94*, edited by L. Gunther and B. Barbara (Kluwer, Dordrecht, 1995).
[2] W. Wernsdorfer and R. Sessoli, Science **284**, 133 (1999).
[3] A.L. Barra, P. Debrunner, D. Gatteschi, C.E. Schulz, and R. Sessoli, Europhys. Lett. **35**, 133 (1996).
[4] C. Sangregorio, T. Ohm, C. Paulsen, R. Sessoli, and D. Gatteschi, Phys. Rev. Lett. **78**, 4645 (1997).
[5] T. Ohm, C. Sangregorio, and C. Paulsen, Eur. Phys. J. B **6**, 195 (1998).
[6] L. D. Landau and E. M. Lifshitz, *Quantum Mechanics*, 3rd ed. (Pergamon, Oxford, 1976), Sec. 90.
[7] D. Loss, D.P. DiVincenzo, and G. Grinstein, Phys. Rev. Lett. **69**, 3232 (1992); J. von Delft and C.L. Henley, *ibid.* **69**, 3236 (1992).
[8] A. Garg, Europhys. Lett. **22**, 205 (1993).
[9] M. Wilkinson, Physica D **21**, 341 (1986). See final paragraph of Sec. 6.
[10] M.V. Berry and M. Wilkinson, Proc. R. Soc. London, Ser. A **392**, 15 (1984).
[11] G. Herzberg and H.C. Longuet-Higgins, Discuss. Faraday Soc. **35**, 77 (1963).
[12] M. Stone, Kee-Su Park, and A. Garg, J. Math. Phys. **41**, 8025 (2000).
[13] A. Caneschi, D. Gatteschi, and R. Sessoli, J. Am. Chem. Soc. **113**, 5873 (1991); R. Sessoli, D. Gatteschi, A. Caneschi, and M.A. Novak, Nature (London) **365**, 141 (1993).
[14] J. Friedman, M.P. Sarachik, J. Tejada, and R. Ziolo, Phys. Rev. Lett. **76**, 3830 (1996).
[15] L. Thomas *et al.*, Nature (London) **383**, 145 (1996).
[16] J.A.A.J. Perenboom, J.S. Brooks, S. Hill, T. Hathaway, and N.S. Dalal, Phys. Rev. B **58**, 330 (1998).
[17] A.L. Barra, D. Gatteschi, and R. Sessoli, Phys. Rev. B **56**, 8192 (1997).
[18] A short review is given by B. Barbara, L. Thomas, F. Lionti, I. Chiorescu, and A. Sulpice, J. Magn. Magn. Mater. **200**, 167 (1999).
[19] See, e.g., the review by A. Caneschi *et al.*, J. Magn. Magn. Mater. **200**, 182 (1999).
[20] Ersin Keçecioğlu and A. Garg, Phys. Rev. B **63**, 064422 (2001).
[21] R B. Dingle and G.J. Morgan, Appl. Sci. Res. **18**, 221 (1967); **18**, 238 (1967).
[22] K. Schulten and R.G. Gordon, J. Math. Phys. **16**, 1971 (1975).
[23] P.A. Braun, Teor. Mat. Fizika **37**, 355 (1978) [Theor. Math. Phys. **37**, 1070 (1978)]; P.A. Braun, Rev. Mod. Phys. **65**, 115 (1993).
[24] J.L. van Hemmen and A. Sütő, Europhys. Lett. **1**, 481 (1986); Physica B **141**, 37 (1986).
[25] A. Garg, J. Math. Phys. **39**, 5166 (1998).
[26] A. Garg, Phys. Rev. Lett. **83**, 4385 (1999).
[27] A. Garg, math-ph/0003005 (unpublished).
[28] A. Garg, Phys. Rev. B **64**, 094413 (2001); **64**, 094414 (2001).
[29] J. Villain and A. Fort, Eur. Phys. J. B **17**, 69 (2000).
[30] F. Hartmann-Boutron, J. Phys. I **5**, 1281 (1995); A. Garg, Europhys. Lett. **50**, 382 (2000).
[31] W. Wernsdorfer (private communication).
[32] I. Tupitsyn and B. Barbara, cond-mat/0002180 (unpublished). See pp. 15–17, and Figs. 13–15.
[33] S.P. Kou, J.Q. Liang, Y.B. Zhang, and F.C. Pu, Phys. Rev. B **59**, 11 792 (1999); R. Lu *et al.*, *ibid.* **61**, 14 581 (2000); Y.H. Jin *et al.*, *ibid.* **62**, 3316 (2000); R. Lu *et al.*, *ibid.* **62**, 3346 (2000); S.K. Yoo and S.Y. Lee, *ibid.* **62**, 5713 (2000); R. Lu, J.L. Zhu, Y. Zhou, and B.-L. Gu, *ibid.* **62**, 11 661 (2000); J.L. Zhu *et al.*, Eur. Phys. J. B **16**, 507 (2000).
[34] V.V. Ulyanov and O.B. Zaslavskii, Phys. Rep. **216**, 179 (1992).
[35] This method is one of the commonest and most efficient for solving matrix eigensystems. See, e.g., W. H. Press, B. P. Flannery, S. A. Teukolsky, and W. T. Vetterling, *Numerical Recipes* (Cambridge University Press, Cambridge, UK, 1986), Chap. 11.
[36] See EPAPS Document No. E-PRBMDO-65-044206 for 12 pages of tables. Table I herein lists all the underlying polynomials along with their zeros, and Table II lists all the diabolical points for the Mn_{12}-ac system, as calculated by our perturbative method as well as by numerical diagonalization. This document may be retrieved via the EPAPS homepage (http://www.aip.org/pubservs/epaps.html) or from ftp.aip.org in the directory /epaps/. See the EPAPS homepage for more information.
[37] This result also stems from the fourth-order term since it only allows transitions between energy levels with $\Delta m = 4p$, where p is an integer. For spin S the existence of the ground state tunneling requires $2S = 4p$, as before.
[38] This field value, along with some other important ones, is listed in Table I.
[39] The lower bounds for x_1 and x_3 are found by noting that they arise at $h_x = 0$, since for any fixed m, the curve for $f(x)$ shifts upward as h_x is reduced. The lower bound for x_2 (and upper bound for x_3) follows from the fact that $f'(x) = 0$ at $x = -1/\sqrt{6}$.
[40] By writing U_0 and $U_{*2,3} = U_i$, we do not mean that these three critical energies are equal, but that they lie *inside* the classically allowed region.
[41] M.V. Berry and K.E. Mount, Rep. Prog. Phys. **35**, 315 (1972).
[42] A more rigorous argument is given in V. I. Arnold, *Mathematical Methods of Classical Mechanics* (Springer-Verlag, New York, 1978), Appendix 10.
[43] Consider the polynomial $(x-a_1)(x-a_2)\cdots(x-a_n)$, where the a_i are all positive. The coeffcient of x^{n-k} is $(-1)^k$ times the symmetric sum $\Sigma a_{i_1} a_{i_2} \cdots a_{i_k}$ of all distinct k-fold products of the a's.
[44] M.V. Berry, Proc. R. Soc. London, Ser. A **392**, 45 (1984).
[45] M.V. Berry and R.J. Mondragon, J. Phys. A **19**, 873 (1986).
[46] The considerations of this subsection were prompted by a private communication from Dr. Wernsdorfer, informing us that numerical diagonalization with the Mn_{12}-ac parameters revealed that in addition to being quenched on the h_z axis, the splitting of the $m = -10$ and $m' = 9$ states was also quenched at a very close by point.
[47] Hence, $a = 1.067 \times 10^{-2}$. It seems safe to assume that $c \ll 1$, so that $b \simeq 3 \times 10^{-4}$.